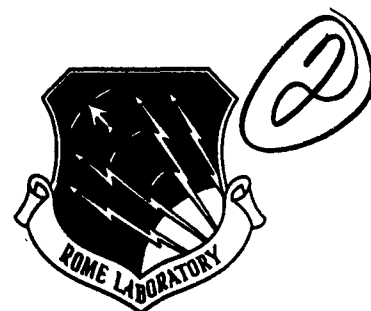


RL-TR-91-167
Final Technical Report
August 1991

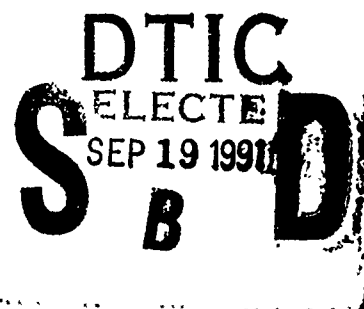
AD-A240 822



STRESS AND THERMAL STRESS COMPENSATION IN QUARTZ SAW DEVICES

Laboratoire De Physique Et Metrologie Des Oscillateurs

E. Bigler, D. Hauden, S. Ballandras



APPROVED FOR PUBLIC RELEASE; DISTRIBUTION UNLIMITED.

91-10794



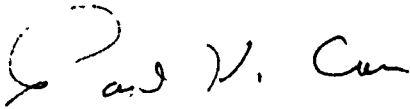
Rome Laboratory
Air Force Systems Command
Griffiss Air Force Base, NY 13441-5700

91 9 17 010

This report has been reviewed by the Rome Laboratory Public Affairs Office (PA) and is releasable to the National Technical Information Service (NTIS). At NTIS it will be releasable to the general public, including foreign nations.

RL-TR-91-167 has been reviewed and is approved for publication.

APPROVED:


PAUL H. CARR
Project Engineer

FOR THE COMMANDER:



JOHN K. SCHINDLER, Director
Electromagnetics & Reliability Directorate

If your address has changed or if you wish to be removed from the Rome Laboratory mailing list, or if the addressee is no longer employed by your organization, please notify RL(ERAC) Hanscom AFB MA 01731-5000. This will assist us in maintaining a current mailing list.

Do not return copies of this report unless contractual obligations or notices on a specific document require that it be returned.

REPORT DOCUMENTATION PAGE

Form Approved
OMB No. 0704-0188

Public reporting burden for this collection of information is estimated to average 1 hour per response, including the time for reviewing instructions, searching existing data sources, gathering and maintaining the data needed, and completing and reviewing the collection of information. Send comments regarding this burden estimate or any other aspect of this collection of information, including suggestions for reducing this burden, to Washington Headquarters Services, Directorate for Information Operations and Reports, 1215 Jefferson Davis Highway, Suite 1204, Arlington, VA 22202-4302, and to the Office of Management and Budget, Paperwork Reduction Project (0704-0188), Washington, DC 20503

| | | | | | |
|--|---|--|-----------------------------------|---|--|
| 1. AGENCY USE ONLY (Leave Blank) | | 2. REPORT DATE August 1991 | | 3. REPORT TYPE AND DATES COVERED Final Jun 87 - May 90 | |
| 4. TITLE AND SUBTITLE STRESS AND THERMAL STRESS COMPENSATION IN QUARTZ SAW DEVICES | | | | 5. FUNDING NUMBERS C - AFOSR 87-0241 PE - 61102F PR - 2305 TA - J5 WU - 48 | |
| 6. AUTHOR(S) E. Bigler, D. Hauden, S. Ballandras | | | | | |
| 7. PERFORMING ORGANIZATION NAME(S) AND ADDRESS(ES) Laboratoire De Physique Et Metrologie Des Oscillateurs Center National de la l'Observatoire 25000 Bensancon, France | | | | 8. PERFORMING ORGANIZATION REPORT NUMBER | |
| 9. SPONSORING/MONITORING AGENCY NAME(S) AND ADDRESS(ES) Rome Laboratory (ERAC) European Office of Aerospace Hanscom AFB MA 01731-5000 Research and Development Box 14 FPO, New York 09510-0200 | | | | 10. SPONSORING/MONITORING AGENCY REPORT NUMBER RL-TR-91-167 | |
| 11. SUPPLEMENTARY NOTES Rome Laboratory Project Engineer: Paul H. Carr/ERAC/(617)377-3686 | | | | | |
| 12a. DISTRIBUTION/AVAILABILITY STATEMENT Approved for public release; distribution unlimited. | | | | 12b. DISTRIBUTION CODE | |
| 13. ABSTRACT (Maximum 200 words) In Surface Acoustic Waves (SAW) devices, the external perturbations induce static or quasi-static stresses and strains within the crystal, which by nonlinear coupling modify the phase velocity and therefore induce frequency shifts in SAW oscillators. Highly stabilized SAW oscillators need to minimize these effects. A theoretical search identified three (3) doubly rotated cuts which are both temperature-compensated and planar-stress compensated. Experimental measurements have been made on the three (3) doubly rotated cuts (including a cut close to B.K. Sinha's STC cut). They were found to be both temperature compensated and mechanically in-plane-compression-compensated. A dynamic thermal experiment showed that these cuts have one tenth the sensitivity of the standard ST-X cut. | | | | | |
| 14. SUBJECT TERMS Service Acoustic Waves | | | | 15. NUMBER OF PAGES 60 | |
| | | | | 16. PRICE CODE | |
| 17. SECURITY CLASSIFICATION OF REPORT UNCLASSIFIED | 18. SECURITY CLASSIFICATION OF THIS PAGE UNCLASSIFIED | 19. SECURITY CLASSIFICATION OF ABSTRACT UNCLASSIFIED | 20. LIMITATION OF ABSTRACT SAR | | |

TABLE OF CONTENTS

| | |
|---|----|
| GENERAL PRESENTATION | 3 |
| 1 - DERIVATION OF STRESS SENSITIVITY COEFFICIENTS FOR SURFACE ACOUSTIC WAVES | 5 |
| 2 - QUARTZ CUTS COMPENSATED FOR BOTH 1st ORDER TEMPERATURE EFFECTS AND PLANAR ISOTROPIC STRESSES EFFECTS | 12 |
| a) Symmetrical in-plane stress distribution in a thin plate | 12 |
| b) 1st order static temperature effects | 12 |
| c) Numerical results for quartz | 13 |
| 3 - EXPERIMENTAL RESULTS : STATIC TEMPERATURE EFFECTS AND MECHANICAL TESTS BY DIAMETRAL COMPRESSION | 15 |
| a) Experimental methods | 15 |
| b) Results for the cuts ($\phi = 0, -13^\circ < \theta < -2.5^\circ, 29^\circ < \Psi < 33^\circ$) and ($\phi = 0, 33^\circ < \theta < 47^\circ, 42^\circ < \Psi < 50^\circ$) | 17 |
| c) Improvements of the model : anisotropic stress calculation, effects of plate thickness | 25 |
| d) Comparison with results obtained by finite element analysis | 27 |
| 4 - EXPERIMENTAL STUDY OF DYNAMICAL TEMPERATURE EFFECTS | |
| a) Experimental method | 31 |
| b) Results for the (ST,X) cut and for the cut ($\phi = 0^\circ, \theta = -7^\circ, \Psi = 31^\circ$) | 32 |
| 5 - CALCULATIONS ON FLEXURAL SENSITIVITY OF SAW QUARTZ CUTS COMPENSATED FOR PLANAR ISOTROPIC STRESSES | 35 |
| a) Classical isotropic stress calculations | 35 |
| b) Anisotropic stress model | 38 |
| c) Numerical results for the cuts (ST,X) and ($\phi = 0; \theta = -10; \Psi = 30$) ($\phi = 0; \theta = 41.8; \Psi = 48.2$) | 41 |
| CONCLUSION | 45 |
| Appendix 1 : Cut angles and propagation direction for SAWs on quartz : Definition and symmetry properties | 47 |

ACKNOWLEDGEMENTS

Contributions to various portions of the program were made by the following staff members of LPMO

Mrs G. Théobald
MM. C. Bonjour
R. Coquerel
R. Prétot

The finite element software has been used by courtesy of LCS's director, Mr. J.M. CROLET.



| Accession For | |
|--------------------|-------------------------------------|
| NTIS GRA&I | <input checked="" type="checkbox"/> |
| DTIC TAB | <input type="checkbox"/> |
| Unannounced | <input type="checkbox"/> |
| Justification | |
| By _____ | |
| Distribution/ | |
| Availability Codes | |
| Dist | Avail and/or Special |
| A-1 | |

STRESS AND THERMAL STRESS COMPENSATION IN QUARTZ SAW DEVICES

GENERAL PRESENTATION

Surface acoustic waves are sensitive to different physical quantities such as temperature, forces, accelerations, ... [1-8]. The external perturbations induce static or quasi-static stresses and strains in the crystal, which by non-linear coupling modify the wave velocity and therefore induce frequency shifts in a SAW device. It is necessary to minimize these effects in the case of SAW oscillators since they are at the origin of most of frequency instabilities. (On the other hand, high sensitivities can be used also for sensor applications).

Static temperature effects may be avoided by the choice of a temperature-compensated cut like the classical ST-cut.

The effects of forces depending closely on the geometry of the device (shape and fixation conditions), one may think to study this problem for each particular device. Another way which is followed in the present work is to investigate the possibility of stress compensation by using the crystal anisotropy properties. (Fig.1)

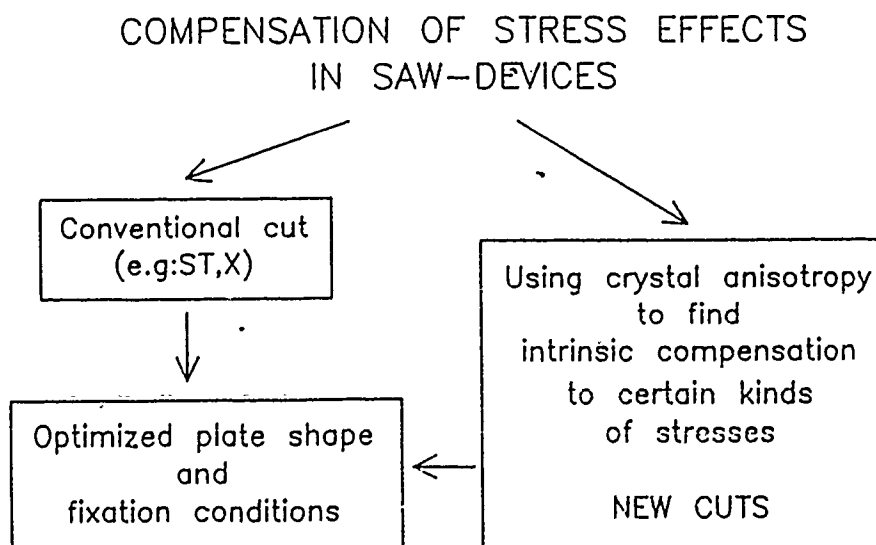


Fig.1 : The problem of stress sensitivity in SAW devices

In this approach [9,10] the effects of stresses are considered as the tensorial equivalent of temperature effects, and under some hypothesis stress sensitivity coefficients can be defined whatever the origin (thermo-elastic effects, external forces) might be. Therefore a general relation between the wave velocity and the six independent components of the quasi-static stress tensor can be given.

Stress compensation will be obtained if the contributions of the main stress components cancel each other, and this may happen for a given distribution of stresses when a suitable SAW quartz cut is found minimizing the velocity shifts. However as a compensation seems unrealistic in the most general case, the problem will be treated first in the case of planar stresses in thin plates, which reduces the number of stress components to three. In addition, a symmetrical stress distribution will be considered, corresponding to equal axial stresses and negligible shear component. In that configuration, stress compensation means that the two in-plane axial stresses induce equal contributions with opposite signs. This approach was used by Eernisse for bulk acoustic wave resonators [11] and led to the development of the famous SC-cut.

The previous analysis, which only takes into account the contribution of in-plane stresses, has been extended using the same formalism to the investigation of flexural sensitivity of quartz cuts. In the case of pure bending, the SAW (which is located close to the surface) will be submitted to compressive in-plane stresses only ; a symmetrical distribution of such bending forces will therefore be equivalent to a symmetrical distribution of compressive, in-plane stresses and will not induce any frequency shift in a SAW cut compensated for planar isotropic stresses.

The present work shows that

- several quartz cuts exist, exhibiting both zero first order temperature coefficient and zero stress coefficient for planar isotropic stresses, according to the model.
- among these cuts exist two singly-rotated quartz plates, and experimental tests were performed to check temperature and stress sensitivity of these particular cuts ; results are compared to theoretical predictions obtained by analytical methods and finite element analysis.
- theoretical calculations on flexural sensitivity of the new cuts (SAW propagating on a bent cantilever beam, on a plate submitted to normal accelerations or on a thin rectangular anisotropic plate) predict a possibility of bending forces compensation if a symmetrical distribution of bending stresses is applied to the device.

1. DERIVATION OF STRESS SENSITIVITY COEFFICIENTS FOR SURFACE ACOUSTIC WAVES

a) Wave propagation in a prestrained medium

The calculation is based on the model proposed by Tiersten [12, 13] for wave propagation in a prestrained medium.

The general equation of a finite amplitude wave of displacement u_i propagating on a medium with specific mass ρ_0 in the natural state submitted to a mechanical bias [12] can be written as

$$\rho_0 \ddot{u}_i = \frac{\partial}{\partial \alpha_k} \left(\overline{A_{iskr}} \frac{\partial u_r}{\partial \alpha_s} \right) \quad (1a)$$

$$N_k \left(\overline{A_{iskr}} \frac{\partial u_r}{\partial \alpha_s} \right) = 0 \text{ on a free surface} \quad (1b)$$

where $\partial/\partial \alpha_k$ refers to the natural-state coordinates, N_k is the cosine director of the normal to the surface. $\overline{A_{iskr}}$ are the modified elastic coefficients resulting from the nonlinear coupling between the static stresses/strains and the high frequency wave. These coefficients can be written in the form

$$\overline{A_{iskr}} = C_{iskr} + \overline{H_{iskr}} \quad (2)$$

where C_{iskr} are the regular second order elastic constants, and $\overline{H_{iskr}}$ appears as a perturbation due to the bias, given by the relation

$$\overline{H_{iskr}} = \delta_{ik} \overline{T_{sr}} + C_{iskruv} \overline{S_{uv}} + C_{iskr} \frac{\partial \overline{U}_i}{\partial \alpha_\ell} + C_{iskr} \frac{\partial \overline{U}_k}{\partial \alpha_\ell} \quad (3)$$

δ_{ik} is the Kronecker symbol, C_{iskruv} are the third order nonlinear elastic constants, $\overline{T_{sr}}$, $\overline{S_{uv}}$ and $\partial \overline{U}_i / \partial \alpha_\ell$ represent respectively the static stresses, strains and displacement gradients characterizing the mechanical bias. (Summation convention on repeated indices is assumed).

b) General expression of SAW velocity

The mechanical displacement corresponding to a SAW propagating in the a_1 direction with a velocity V_0 at an angular frequency ω_0 on an anisotropic medium in

the absence of perturbation, taking piezoelectricity into account, is expressed by

$$u_i^0 = \sum_{r=1}^4 b_i(r) A_r e^{-i\omega_0 \frac{q(r)a_2}{V_0}} e^{i\omega_0 (t - \frac{a_1}{V_0})} \quad (4)$$

The reference axes (a_i) of the natural state are presented in Fig. 2 with respect to the crystal plate.

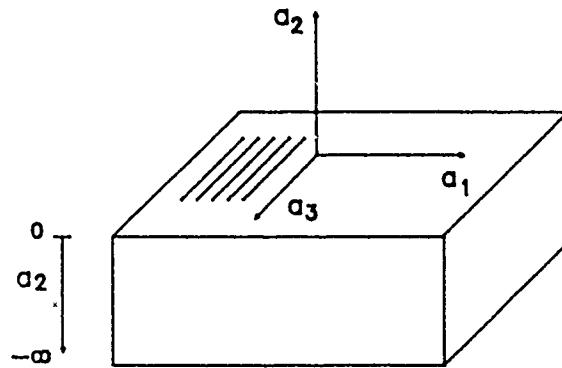


Fig. 2 : Reference axes for a SAW propagating on a semi-infinite crystal plate

$A_r b_i(r)$ represents the amplitudes of the 4 partial waves ($r = 1-4$) of the unperturbed SAW. $q(r)$ is the depth penetration coefficient of the r -th partial wave in the a_2 -direction.

Eq. (4) may be expressed in a closer form by

$$u_i^0 = \sum_{r=1}^4 b_i(r) A_r e^{i\omega_0 [t - (n_1^{(r)} a_1 + n_2^{(r)} a_2) / V_0]} \quad (5)$$

where

$$n_1(r) = 1 \quad n_2(r) = q(r) \quad n_3(r) = 0$$

Applying a perturbation method [13, 14] to the SAW propagating on the constrained crystal (of volume V) the relative velocity shifts $\Delta V/V_0$ can be expressed as

$$\frac{\Delta V}{V_0} = \frac{1}{2\rho_0 \omega_0^2} \frac{\int_V \frac{\partial u_i^0}{\partial a_s} \overline{H_{iskr}} \frac{\partial u_k^0}{\partial a_r} dv}{\int_V u_i^0 u_i^{0*} dv} \quad (6)$$

In this approach, piezoelectricity is taken into account only to determine the unperturbed SAW expressed as a sum of 4 partial waves. The perturbation term $\overline{H_{iskr}}$ is the same as in the non-piezoelectric approximation.

In the most general case, the perturbation terms $\overline{H_{iskr}}$ depend on the space coordinates if the distribution of the static stresses and strains is inhomogeneous, and a particular distribution of stresses is associated with each particular boundary condition. If considering the case of an homogeneous stress and strain distribution eq. (6) takes the simpler form :

$$\frac{\Delta V}{V_0} = \overline{H_{iskr}} U_{iskr} \quad (7)$$

where U_{iskr} depends only on the unperturbed SAW parameters

$$U_{iskr} = \frac{1}{2\rho_0 \omega_0^2} \frac{\int_v \frac{\partial u_i^0}{\partial \alpha_s} \frac{\partial u_k^0}{\partial \alpha_r} dv}{\int_v u_i^0 u_i^{0*} dv} \quad (8)$$

Assuming a plate thickness much greater than the penetration depth of the SAW, the integration of eq. (8) over $a_2 [-\infty, 0]$ yields a similar expression as in [14], except that, taking piezoelectricity into account, summation is made over 4 partial waves

$$U_{iskr} = \frac{1}{2\rho_0 V_0^2} \frac{\sum_{p,q=1}^4 A_p b_k(p) A_q^* b_l^*(q) n_r(p) n_s^*(q) / (q_p - q_q^*)}{\sum_{p,q=1}^4 \frac{A_p b_j(p) A_q^* b_j(q)^*}{q_p - q_q^*}} \quad (9)$$

c) Stress sensitivity coefficients

The perturbing coefficients $\overline{H_{iskr}}$ implicitly contain the dependence between the velocity and the static bias (eq. 3) in term of stresses, strains, and mechanical displacements. The strains can be expressed as function of the stresses by means of the compliance elastic constants s_{uvpq} .

$C_{iskruv} \overline{S_{uv}}$ is written :

$$C_{iskr} \overline{S_{uv}} = C_{iskruv} s_{uvpq} \overline{T_{pq}} \quad (10)$$

The two last terms of eq. (3), $\overline{\partial U_i / \partial a_\ell}$ and $\overline{\partial U_k / \partial a_\ell}$, cannot be, in general, directly expressed as a function of the strains S_{uv} .

But for solving the problem of the static deformations, it is necessary to apply the fixation conditions of the plate. A condition of a fixed point at the origin ($a_1 = a_2 = a_3 = 0$) is first given. A condition of no rigid rotations of the crystal plate around the fixed point may be introduced without loss of generality. This second condition implies

$$\frac{\overline{\partial U_i}}{\overline{\partial a_\ell}} = \frac{\overline{\partial U_\ell}}{\overline{\partial a_i}} \quad \text{for } a_1 = a_2 = a_3 = 0 \quad (11)$$

with as consequence

$$\frac{\overline{\partial U_i}}{\overline{\partial a_\ell}} = \overline{S_{i\ell}} \quad \text{for } a_1 = a_2 = a_3 = 0 \quad (12)$$

Assuming that the SAW propagates in a small volume close to the origin eq. (12) can be considered to be satisfied in this part of the crystal plate. Expanding $\overline{S_{i\ell}}$ in terms of the stresses $\overline{T_{pq}}$, eq. (12) may be expressed close to the origin as

$$\frac{\overline{\partial U_i}}{\overline{\partial a_\ell}} = s_{i\ell pq} \overline{T_{pq}} \quad (13)$$

Combining eqs. (10) and (13) into eq. (3), the velocity shift $\Delta V/V_0$ is obtained in the final form

$$\frac{\Delta V}{V_0} = \overline{T_{pq}} \{ \delta_{ik} \delta_{sp} \delta_{rq} + C_{iskruv} s_{uvpq} + C_{\ell skr} s_{i\ell pq} + C_{is\ell r} s_{k\ell pq} \} U_{iskr} \quad (14)$$

or in a condensed form

$$\frac{\Delta V}{V_0} = \overline{T_{pq}} s_{\alpha pq} \quad (15)$$

where $s_{\alpha pq}$ represent the different stress coefficients. They have the same symmetry as $\overline{T_{pq}}$, i.e. there are six independent stress-sensitivity coefficients.

d) Numerical example for quartz

As it may be seen in eq. (14), the stress sensitivity coefficients depend only on the crystal anisotropy, and are independent of the plate geometry.

They are computed by tensorial contraction on two independent terms :

- the first term is a contraction on 2nd order and 3rd order elastic constants :
 C_{ijkl}, C_{iskruv} .
- the second term U_{iskr} is a combination of terms depending only on the unperturbed SAW parameters.

First, the elastic constants are "rotated" and expressed in the set of axes parallel to the surface, as defined on Figs. 2 and 3. Then the surface wave parameters are computed, taking piezoelectricity into account, using a very classical algorithm, close to Campbell & Jones method [15]. This gives the term U_{iskr} , which is contracted with the first bracket of eq. (14) to give the stress sensitivity coefficients.

An example of numerical results for quartz crystal is given on Fig. 4 where the six independent stress coefficients are plotted on a contour-line map, as a function of cut angles θ , Φ and propagation direction of the SAW Ψ . These angles, defined according to IEEE standard [16] are represented on Fig. 3. This corresponds to a $(YXw\ell t)\Phi\theta\Psi$ plate, SAW propagation in the ℓ -direction.

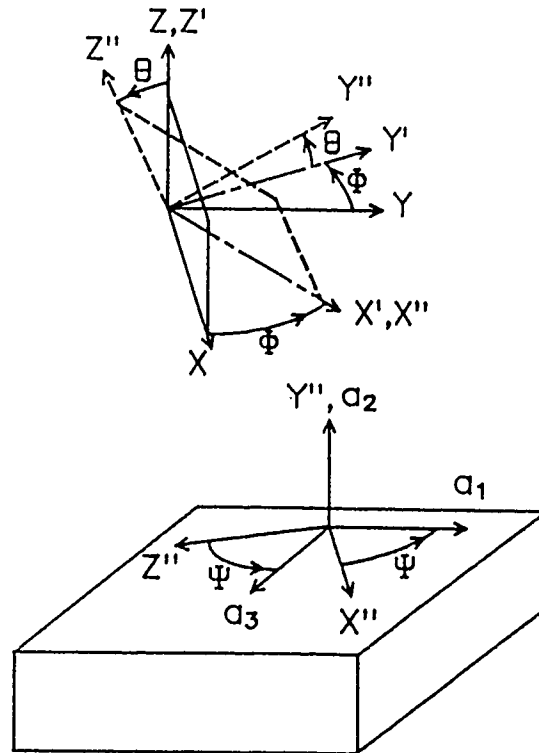


Fig. 3 : Definition of the cut angles Φ , θ and propagation direction Ψ

Correspondance with Euler angles [17] is the following :

$$\lambda_{\text{Euler}} = \Phi_{\text{IEEE}}$$

$$\mu_{\text{Euler}} = \theta_{\text{IEEE}} - 90^\circ$$

$$\theta_{\text{Euler}} = \Psi_{\text{IEEE}}$$

Examples

(for a detailed discussion of the definition of cut angles and symmetry properties of quartz, see Appendix 1).

| cut | Euler | IEEE |
|-----------------|--|---|
| Y-cut, X prop. | $(\lambda = 0, \mu = 90^\circ, \theta = 0)$ | $(\phi = 0, \theta = 0, \Psi = 0)$ equivalent for SAWs to $(\phi = 0, \theta = 180^\circ, \Psi = 0)$ |
| ST-cut, X prop. | $(\lambda = 0, \mu = 132,75^\circ, \theta = 0)$ | $(\phi = 0, \theta = 42,75^\circ, \Psi = 0)$ equivalent for SAWs to $(\phi = 0, \theta = 222,75^\circ, \Psi = 0)$ |
| X-33 cut | $(\lambda = 90^\circ, \mu = 90^\circ, \theta = 33,44^\circ)$ | $(\phi = 90^\circ, \theta = 180^\circ, \Psi = 33,44^\circ)$ equivalent for SAWs on quartz to $(\phi = -90^\circ, \theta = 0, \Psi = 33,44^\circ)$ |

Numerical computation is performed using FORTRAN-77 programs on a DATA GENERAL MV 1500/100 computer. Elastic, piezoelectric and dielectric constants are taken from Slobodnick [17], Bechmann [18] and Thurston [19].

A complete mapping (Fig. 4) $0^\circ < \theta < 90^\circ$ (5° steps) and $-60^\circ < \Phi < 60^\circ$ (5° steps) requires 19×25 values and takes about 15 minutes of CPU Time.

Values of cut angles non represented on Fig. 4 may be found according to symmetry properties of SAWs on quartz (see Appendix 1)

$$s_{a_{pq}}(\phi, \theta, -\Psi) = s_{a_{pq}}(-\phi, \theta, \Psi) \quad (16)$$

$$s_{a_{pq}}(\phi, -\theta, \Psi) = s_{a_{pq}}(180^\circ - \phi, \theta, \Psi) \quad (17)$$

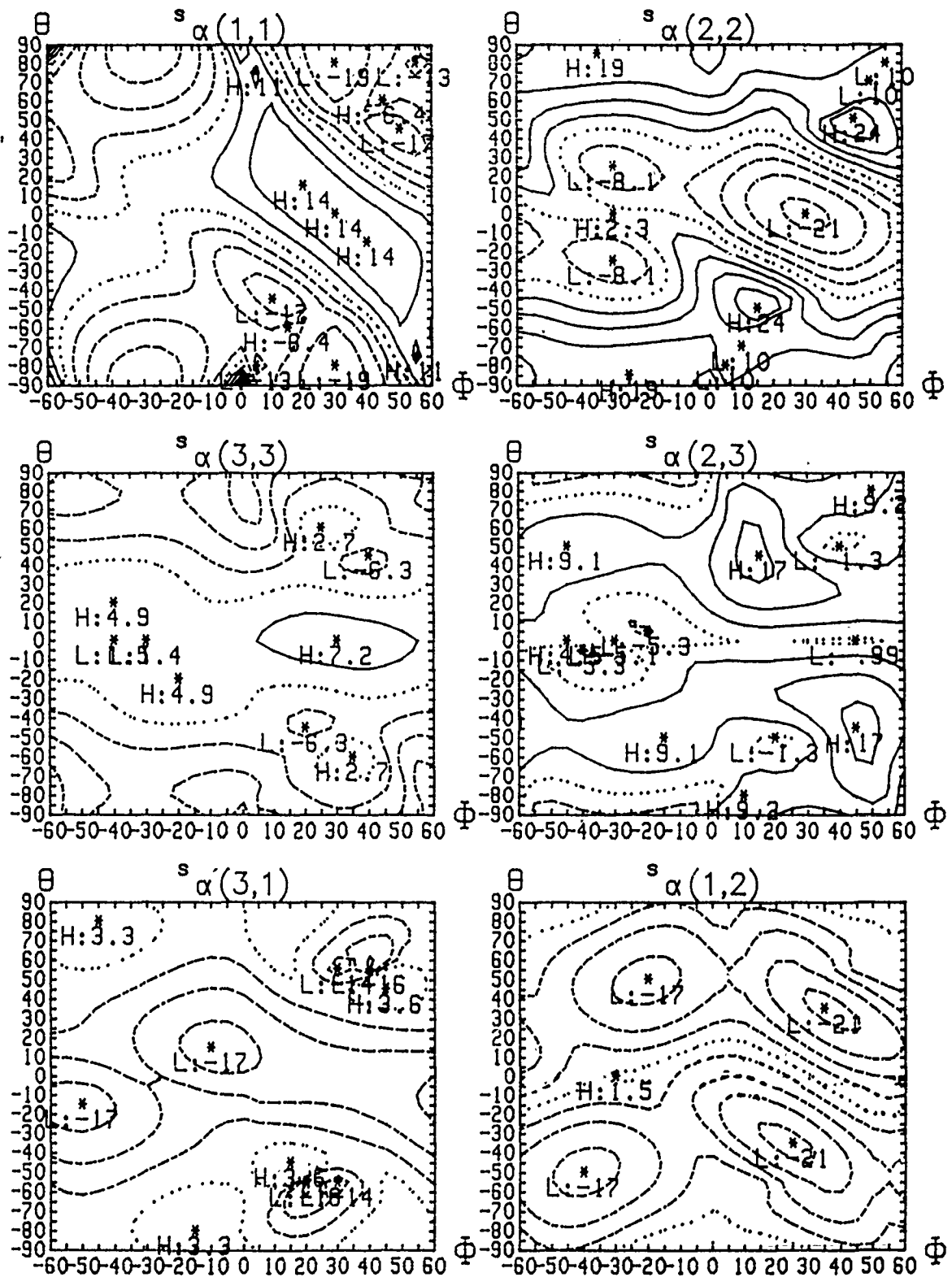


Fig. 4

Example of numerical results for stress coefficients
 Contour-line mapping for SAWs on Quartz, propagation angle $\psi = 30^\circ$
 Piezoelectricity of the crystal is taken into account
 units: $10^{-12} \text{ m}^2 \cdot \text{N}^{-1}$. Contour lines interval: $5 \times 10^{-12} \text{ m}^2 \cdot \text{N}^{-1}$
 solid lines — $s_\alpha > 0$ dotted lines $s_\alpha = 0$ broken lines ---- $s_\alpha < 0$

2. QUARTZ CUTS COMPENSATED FOR BOTH 1st ORDER TEMPERATURE EFFECTS AND PLANAR ISOTROPIC STRESSES EFFECTS

In this section, the model of stress sensitivity coefficients is applied to the problem of planar, isotropic stress compensation. Sensitivity to static temperature effects has also to be taken into account, to define SAW quartz cuts with low stress and temperature sensitivity.

a) Symmetrical in-plane stress distribution in a thin plate

The case of a thin plate of quartz with the main surfaces free of stresses will be considered now. In this case, there is a planar stress distribution of components \overline{T}_{11} , \overline{T}_{33} and \overline{T}_{31} expressed in the set of axes parallel to the surface (Figs. 2 and 3).

An additional symmetry condition will be assumed : $\overline{T}_{11} = \overline{T}_{33}$, $\overline{T}_{13} = 0$. This corresponds to a planar isotropic stress distribution which for instance appears in the problem of thermal stresses in a circular plate. With these assumptions, the velocity shifts depend only on a single stress coefficient s_a

$$\frac{\Delta V}{V_o} = s_a \cdot \overline{T} \quad (18)$$

where $\overline{T} = \overline{T}_{11} = \overline{T}_{33}$ and $s_a = s_{a11} + s_{a33}$

Compensation of planar isotropic stresses using quartz anisotropy consists in finding SAW quartz cuts (ϕ, θ, ψ) satisfying

$$(s_{a11} + s_{a33})(\phi, \theta, \psi) = 0 \quad (19)$$

b) 1st order static temperature effects

Static temperature sensitivity will be defined here using the temperature coefficients of fundamental elastic constants according to H.F. Tiersten and B.K. [1, 12].

he same formalism as in sec. 1, the first order temperature coefficient θ_a is for a pure thermal bias in a free-expanding plate as

$$\frac{\Delta V}{V_o} = \theta_a (0 - \theta_o) \quad (20)$$

where

$$\theta_a = \{C_{iskruv} \ell_{uv} + C_{qskr} \ell_{iq} + C_{isqr} \ell_{kq} + \frac{d}{d\theta} (C_{iskr})\} U_{iskr} \quad (21)$$

and $(\theta - \theta_0)$ is the temperature elevation with respect to the reference state.

In eq. (21) ℓ_{uv} are the coefficients of linear expansion, $d(C_{iskr})/d\theta$ are the first derivatives of the fundamental elastic constants, and U_{iskr} is the combination of SAW parameters defined in the perturbation method for an homogeneous distribution of stresses [10].

c) Numerical results for quartz

The loci of stress-compensated cuts are defined according to eq. (19). Taking the propagation angle ψ as a parameter, these loci are represented on Fig. 5 in the (θ, ϕ) plane in solid lines for different propagation directions : $\psi = 30^\circ$ (Fig. 5a), $\psi = 45^\circ$ (Fig. 5b). On the same graphs are represented in broken lines the loci of zero first-order temperature coefficients.

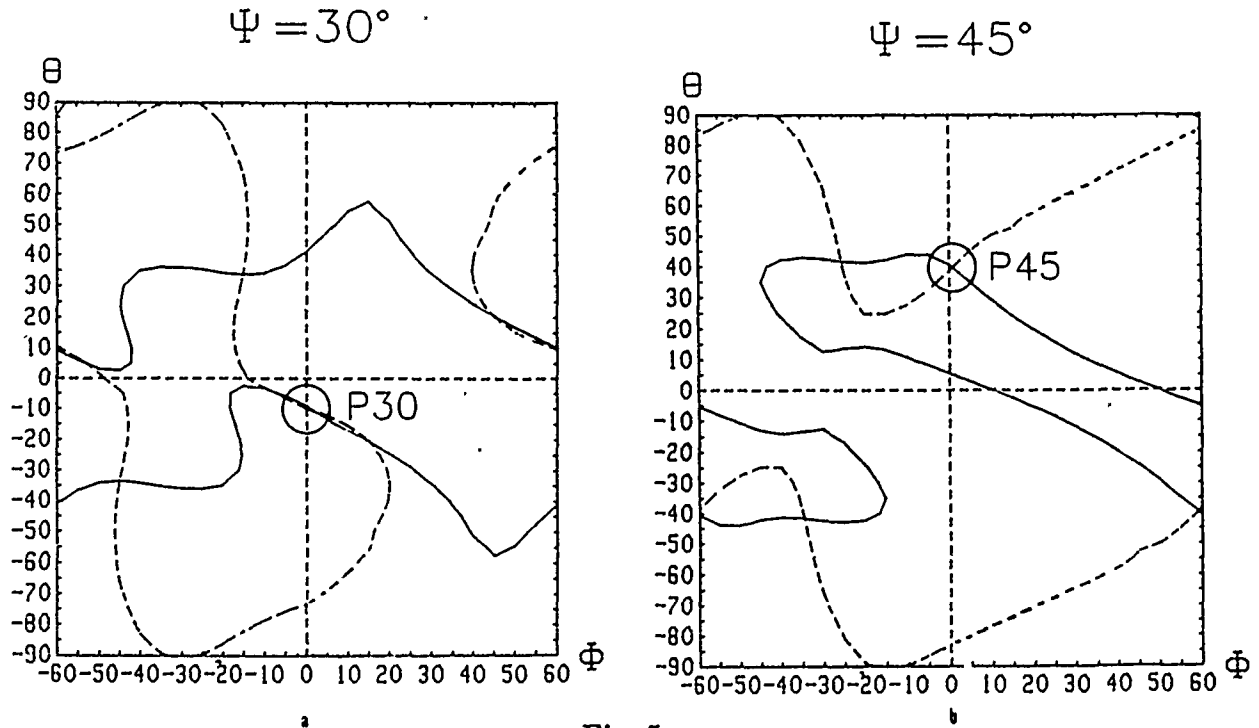


Fig. 5

Solid lines : locus of quartz cuts compensated for planar isotropic stresses effects
 dotted lines : locus of zero first order temperature coefficient
 cut angles θ , ϕ and propagation direction ψ correspond to a $(YXw\ell t)\phi\theta\psi$ plate
 SAW propagation in the ℓ -direction, according to IEEE standard [16]
 Piezoelectricity taken into account

The intersections between the two loci define quartz cuts satisfying both conditions of stress and temperature compensation. Such intersections have been found to exist for angles ψ between 20° and 60° approximately.

In the case of surface waves, the additional parameter ψ (if compared to bulk waves) allows a degree of freedom in the choice of stress- and temperature-compensated cuts. As a first criterium to choose between the different intersection points shown on Fig. 5, it is interesting to look for singly rotated quartz plates ($\phi = 0$) since machining tolerances are easier to obtain than for doubly rotated plates.

The loci of temperature- and stress-compensated cuts are represented on Fig. 6 for singly rotated cuts ($\phi = 0$).

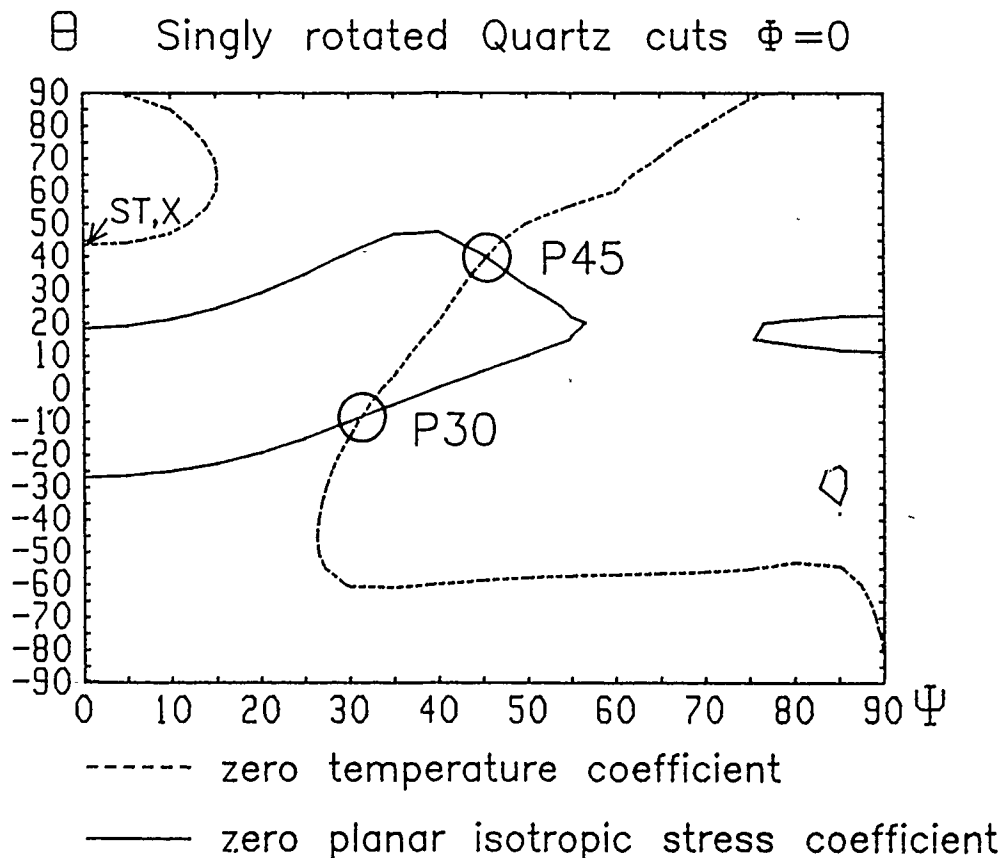


Fig. 6

Solid lines : locus of quartz cuts compensated for planar isotropic stresses effects.

Broken lines : locus of zero first order temperature coefficient

Cut angles ϕ, θ and propagation direction ψ correspond to a $(YXw\ell t) \phi\theta\psi$ plate
 SAW propagation in the ℓ -direction according to IEEE standard 1949 [16]
 Piezoelectricity taken into account

Two intersections exist

- for ψ close to 30° (point P30)
- for ψ close to 45° (point P45)

This last cut (P45 : $\phi = 0, \theta = 45^\circ, \psi = 45^\circ$) is close to B.K. Sinha's STC-cut [20] ($\phi = 0, \theta = 41.8^\circ, \psi = 46.89^\circ$).

In order to check the model presented here, experimental work has been performed on these two cuts, as exposed now.

3. EXPERIMENTAL RESULTS

a) Experimental method

Experiments are performed on quartz delay lines (100 and 150 finger pairs, transducer period : $34 \mu\text{m}$, time delay = $1.5 \mu\text{s}$) built on circular plates (diameter : 22 mm, thickness : 1 mm or 2 mm). The device is used in an oscillator operating at 100 Mhz.

Temperature compensation is checked by plotting the frequency vs temperature curve between -20°C and $+50^\circ\text{C}$. The propagation angle ψ is adjusted to keep the inversion point of the frequency/temperature curve between 18°C and 25°C .

When temperature compensation has been found, the delay line is submitted to mechanical stresses with an apparatus represented on Fig. 7.

The circular plate is submitted to a single or double diametral compression obtained by two pairs of knife-edges acting at 90° to each other.

The plate may be rotated around its axis, and the force-frequency effect is measured for each azimuthal angle β between the propagation direction of the SAW and the direction of the force (Fig. 7).

The experimental procedure is as follows :

The knife-edges are removed, and the plate is held by a clamp until a new angular position is set. The plate is then submitted to a diametral pre-compression of about 1N. The clamp is removed, so that the plate is submitted only to the compressive forces. An additional force between 1N and 10N is set, and the frequency shifts are measured with respect to the pre-strained state. The azimuthal angle is measured without contact by optical means.

The force-frequency effect in a circular disk may be derived from the stress sensitivity coefficients and from the classical theory of elasticity [21].

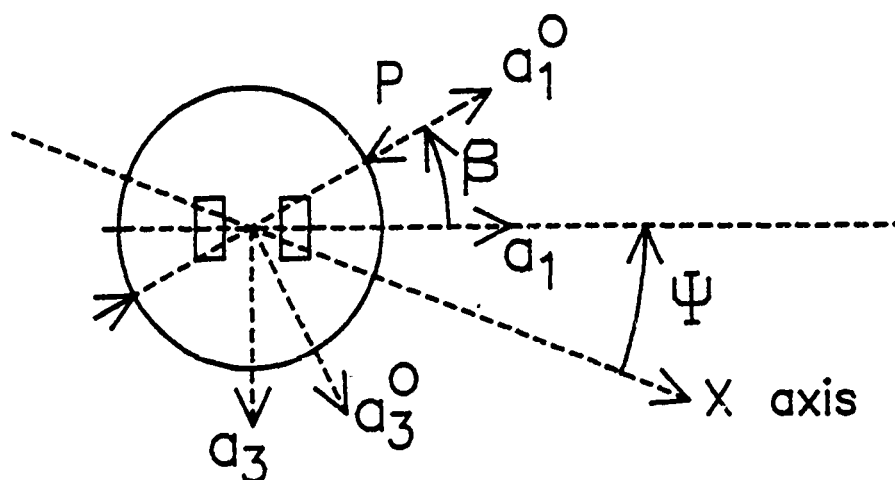


Fig:7 : Experimental setup for single and symmetrical diametral compression of a circular quartz delay line

The stress components at the center of an isotropic disk (diameter d , thickness t) submitted to a single diametral compression by a force P are expressed as

$$\overline{T}_{11}^o = -\frac{6P}{\pi dt}, \quad \overline{T}_{33}^o = +\frac{2P}{\pi dt}, \quad \overline{T}_{13}^o = 0 \quad (23)$$

where upper index "o" refers to a set of axes (a_1^o, a_3^o) parallel to the direction of the force (Fig. 7).

After rotation to a set of axes (a_1, a_3) parallel to the direction of the SAW, the relative velocity shifts may be expressed in the final form

$$\frac{\Delta F}{F_o} = -\frac{2P}{\pi dt} \left((s_{a_{11}} + s_{a_{33}}) + 2(s_{a_{11}} - s_{a_{33}}) \cos 2\beta - 2s_{a_{13}} \sin 2\beta \right) \quad (22)$$

Eq. (23) shows that the angular dependence of the frequency shifts is sinusoidal, with an offset value of $(-2P/\pi dt) (s_{a_{11}} + s_{a_{33}})$ corresponding to the case of a symmetrical compression with two orthogonal forces of magnitude $P/2$.

**b) Results for the cuts ($\phi = 0, -13^\circ < \theta < -2.5^\circ, 29^\circ < \psi < 33^\circ$)
and ($\phi = 0, 37^\circ < \theta < 47^\circ, 42^\circ < \psi < 50^\circ$).**

Temperature effects

Singly-rotated cuts in the vicinity of the P30 cut were tested with cut angles $\theta = -2.5^\circ, -5^\circ, -7^\circ, -10^\circ, -13^\circ$, and the propagation angles ψ corresponding to an inversion point at room temperature were found at $32.5^\circ, 31.5^\circ, 31^\circ, 30^\circ, 29^\circ$ respectively (Figs. 8 and 9). As a reference, the theoretical curve $(-34 \times 10^{-9} \text{ ppm.K}^{-2})$ for the classical ST,X cut is shown. It may be seen that the thermal behavior of the new cuts is very similar to the classical ST,X cut. In the vicinity of the P45 cut, four singly-rotated cuts ($\phi = 39^\circ, \psi = 46^\circ; \theta = 33^\circ, \psi = 44.3^\circ; \theta = 41.8^\circ, \psi = 48.2^\circ; \theta = 45^\circ, \psi = 47^\circ$) were tested. Results appear on Figs. 10 and 11.

Temperature-compensated cuts were experimentally found close to the theoretical values ($|\psi_{\text{theory}} - \psi_{\text{exp}}| < 0.5^\circ$) in the vicinity of the P30 cut. The difference between theory and experiment is greater (about 2°) in the vicinity of the P45 cut, and the corrections introduced by the piezoelectric model do not cancel this discrepancy existing also in the non-piezoelectric approximation used before.

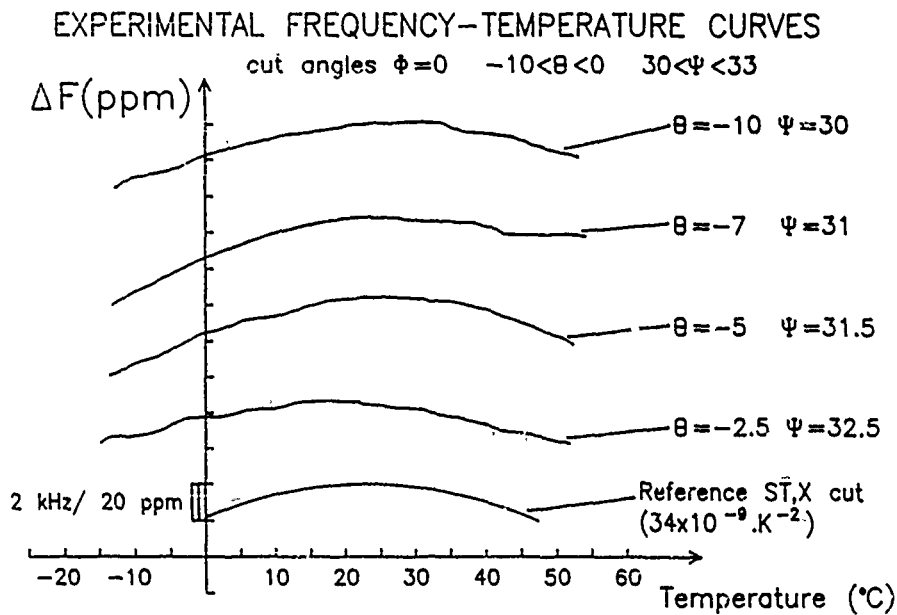


Fig. 8 : Experimental static temperature characteristics for the cuts
 $(\phi = 0, -13^\circ < \theta < -2.5^\circ, 29^\circ < \psi < 33^\circ)$
 Comparison with the classical ST,X cut

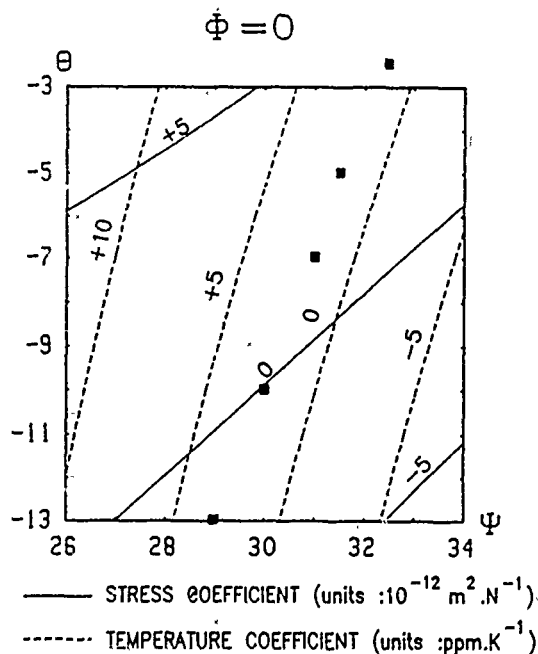


Fig. 9 :
 Theoretical contour line maps of temperature and planar isotropic stress coefficients
 These curves are used as a guide line to experiment real quartz cuts
 in the vicinity of the intersection of both zero-stress and zero-temperature effects
 cut angles : $\phi = 0, -13^\circ < \theta < -2.5^\circ$
 propagation direction : $26^\circ < \psi < 34^\circ$
 ■ = real cuts, experimentally found temperature-compensated
 and measured in the mechanical stress experiment

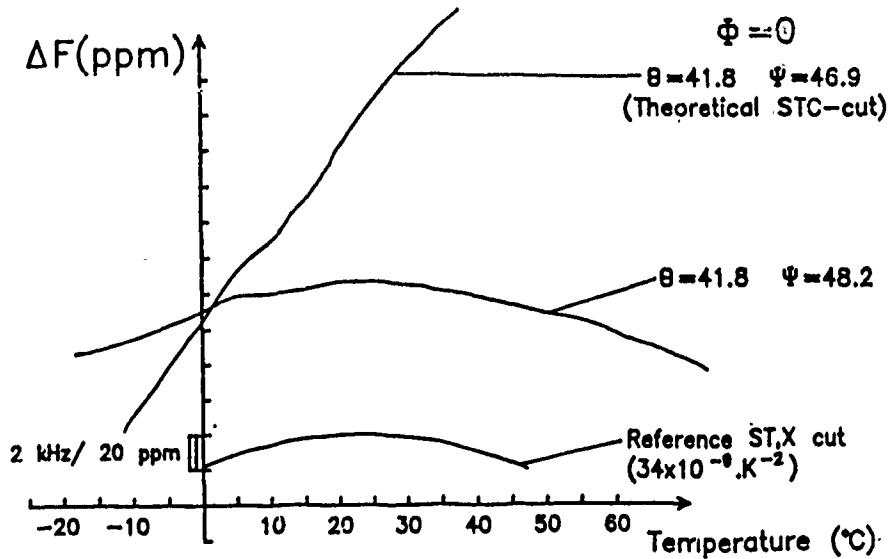


Fig. 10

Experimental static temperature characteristics

- a - for the cut ($\phi = 0, \theta = 41.8^\circ, \psi = 46.9^\circ$) corresponding to the theoretical values of B.K. Sinha's STC cut [14]
 b - for the corrected cut ($\phi = 0, \theta = 41.8^\circ, \psi = 48.2^\circ$) close to the STC cut

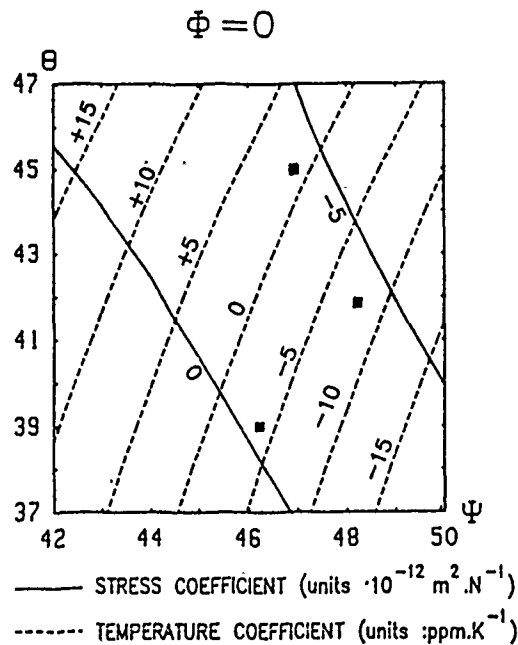


Fig. 11

Theoretical contour line maps of temperature and planar isotropic stress coefficients

These curves are used as a guide line to experiment real quartz cuts in the vicinity of the intersection of both zero-stress and zero-temperature effects

cut angles: $\phi = 0, 37^\circ < \theta < 47^\circ$

propagation direction: $42^\circ < \psi < 50^\circ$

■ = real cuts, experimentally found temperature-compensated and measured in the mechanical stress experiment

In the neighborhood of the P45 cut, the sensitivity of temperature-compensation to the propagation angle ψ is about $-3.5 \text{ ppm/}^\circ\text{C}$ for an increment of $+1^\circ$ on ψ . This figure is higher than for the P30 cut ($\phi = 0, \theta = -10^\circ, \psi = 30^\circ$): $-2.5 \text{ ppm/}^\circ\text{C}$ for $\Delta\psi = +1^\circ$.

Second-order temperature coefficient is very similar for the two cuts, i.e. about $(-34 \times 10^{-9} \text{ ppm.K}^{-2})$. The theoretical value predicted by Sinha [20] for the STC cut is $(-9 \times 10^{-9} \text{ ppm.K}^{-2})$ which does not correspond to our experimental results.

In the neighbourhood of this cut, the sensitivity of temperature-compensation to the propagation angle ψ is about $-3.5 \text{ ppm/}^\circ\text{C}$ for an increment of $+1^\circ$ on ψ . This figure is higher than for the cut ($\phi = 0, \theta = -10^\circ, \psi = 30^\circ$): $-2.5 \text{ ppm/}^\circ\text{C}$ for $\Delta\psi = +1^\circ$.

Force-frequency effect

Figures 12, 13 and 14 show a comparison between experimental data and the theoretical curves computed from the following values (Table I).

Stress compensation effects are clearly shown when the circular delay lines are submitted to a pair of orthogonal forces of the same magnitude. But in the case of a single diametral compression, the experimental points do not exactly match the theoretical sinusoidal curve (Fig. 12). The reasons of this discrepancy might be either a systematic error due to parasitic stresses induced by the experimental setup, or due to the fact that the dimensions of the delay ($9.5 \times 4.5 \text{ mm}^2$) are not small with respect to the diameter of the plate (22 mm).

To investigate the possible origin of the discrepancy, the following attempts were made :

- using stress calculation taking anisotropy into account
- increasing plate thickness to check the influence of parasitic bending forces.
- reducing bias introduced by systematic calculation.

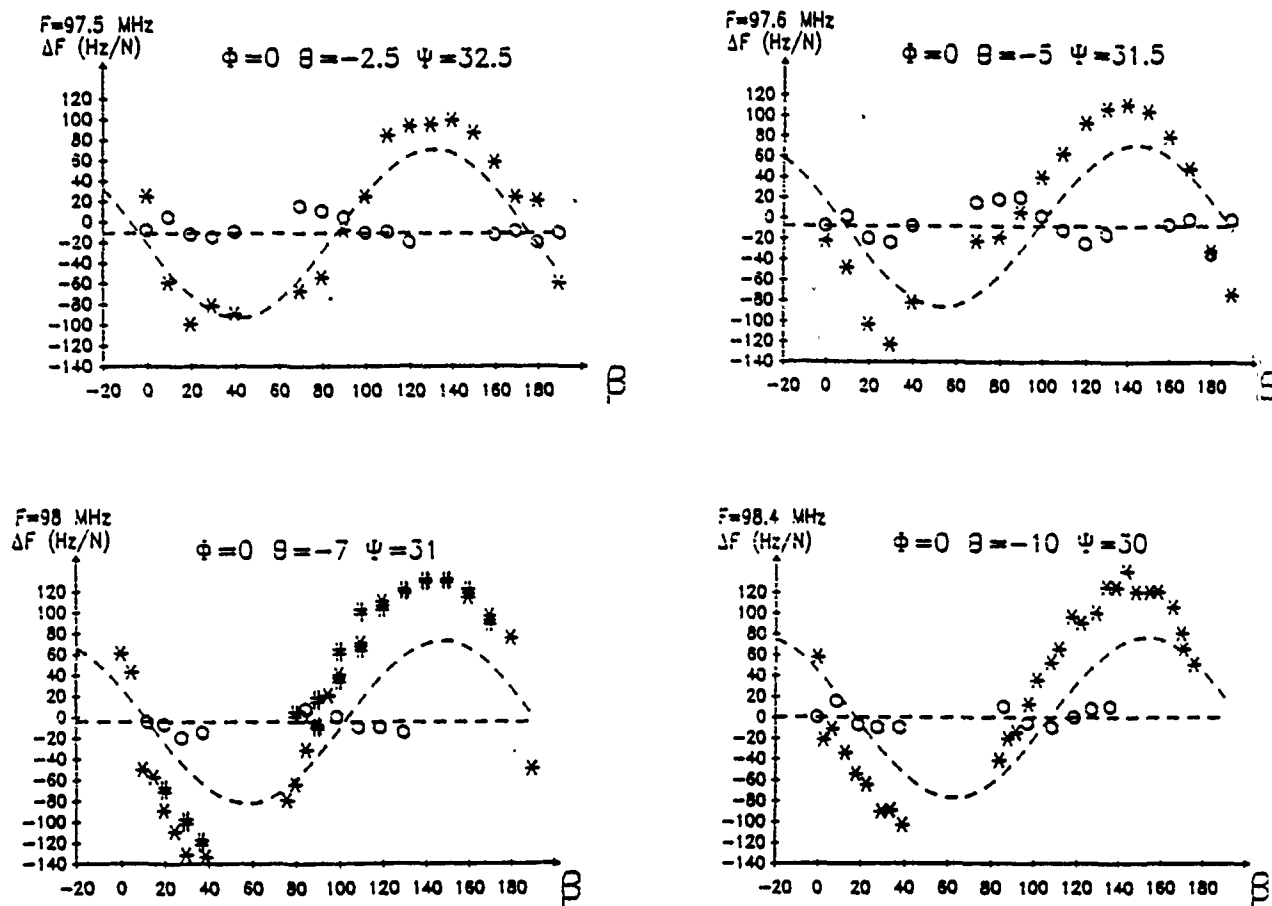


Fig. 12

Experimental force-frequency effect on temperature-compensated circular quartz delay lines with a low sensitivity to planar isotropic stresses:

$$\Phi = 0 \quad -10^\circ < \theta < -2.5^\circ \quad 30^\circ < \psi < 33^\circ$$

single diametral compression : * represents experimental values
solid sinusoidal curve : theoretical values

double diametral compression : o represents experimental values
dashed horizontal line : theoretical values

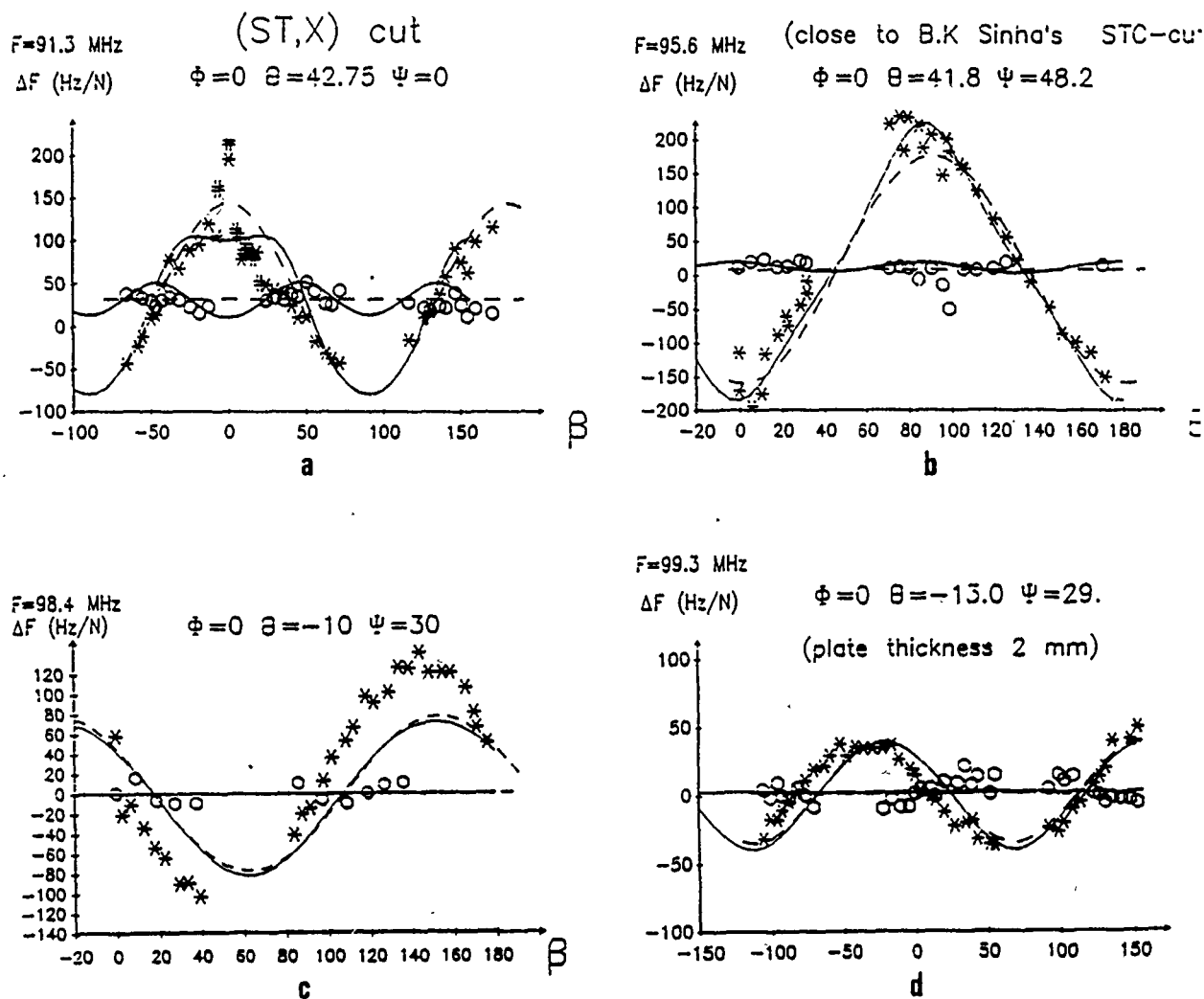


Fig. 13

Experimental results of the force-frequency effect

solid lines : anisotropic stress model

broken lines : isotropic stress model

a : (ST,X) cut

b : ($\phi = 0$, $\theta = 41.8^\circ$, $\psi = 48.2^\circ$) close to STC cut

c : ($\phi = 0$, $\theta = -10^\circ$, $\psi = 30^\circ$)

a, b and c : plate thickness 1 mm

d : ($\phi = 0$, $\theta = -13^\circ$, $\psi = 29^\circ$) plate thickness : 2 mm

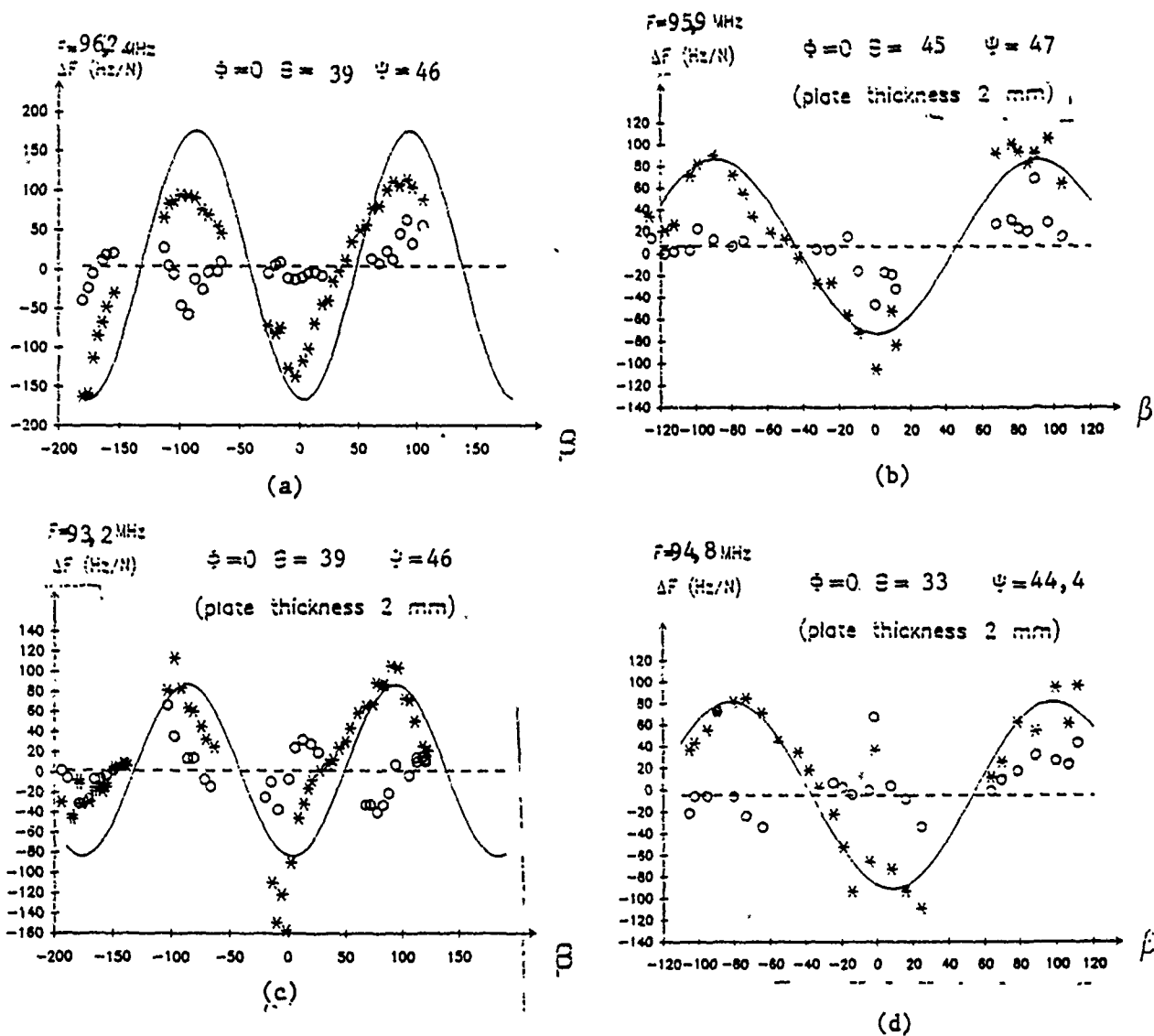


Fig. 14

Experimental results of the force-frequency effect in the vicinity of P45 cut

solid lines : single diametral compression

broken lines : double diametral compression

a : ($\phi=0$, $\theta=39$, $\psi=46$) plate thickness : 1 mm

b : ($\phi=0$, $\theta=45$, $\psi=47$)

c : ($\phi=0$, $\theta=39$, $\psi=46$) plate thickness : 2 mm

d : ($\phi=0$, $\theta=33$, $\psi=44.4$)

| $\phi = 0$ | Theoretical values of stress coefficient units : $10^{-12} \text{ m}^2 \cdot \text{N}^{-1}$ | | | Theoretical values of frequency shifts Isotropic stress calculation $(\Delta f/f_0) \cdot (A/P)$ units : $10^{-12} \text{ m}^2 \cdot \text{N}^{-1}$ A : diameter \times thickness P : applied diametral load (1 N) | | | Thickness (mm) | Frequency f_0 (MHz) | Predicted values of force-frequency effect Δf (Hz) |
|------------|--|---------------|---------------|---|--|--|-------------------|--------------------------|---|
| 0 | ψ | $s_{\phi 11}$ | $s_{\phi 33}$ | $s_{\phi 13}$ | | | | | |
| -2.5 | 32.5 | 0.8 | 2.7 | -14.3 | -2.2 - 2.7 cos 2β + 18.2 sin 2β | | 1 | 97.5 | -9.75 - 11.97 cos 2β - 80.7 sin 2β |
| 5 | 31.5 | -0.8 | 3.2 | -13.3 | -1.5 + 5.1 cos 2β - 16.9 sin 2β | | 1 | 97.6 | -6.65 + 22.6 cos 2β - 75 sin 2β |
| -7 | 31 | -2.1 | 3.4 | -12.5 | -0.83 + 7 cos 2β - 15.9 sin 2β | | 1 | 98.1 | -3.7 + 31.2 cos 2β - 70.9 sin 2β |
| -10 | 30 | 3.9 | 3.6 | -11.1 | 0.2 + 9.6 cos 2β - 14.1 sin 2β | | 1 | 98.3 | 0.9 + 42.9 cos 2β - 63 sin 2β |
| 13 | 29 | -5.6 | 3.8 | -9.7 | 1.15 + 12 cos 2β - 12.4 sin 2β | | 2 | 99.3 | 2.6 + 27.1 cos 2β - 28 sin 2β |
| 41.8 | 48.2 | 12.8 | -17.4 | 0.54 | 2.9 - 38.5 cos 2β + 0.7 sin 2β | | 1 | 95.6 | 12.6 - 167.3 cos 2β + 3.04 sin 2β |
| 42.75 | 0 (ST) | -16.8 | 4.4 | 0 | 7.9 + 27 cos 2β | | 1 | 91.3 | 32.8 + 112.05 cos 2β |
| 39 | 46 | 15.1 | -6.71 | -3.8 | 0.485 - 19.6 cos 2β - 2.5 sin 2β | | 2 | 95.2 | 2.1 - 85 cos 2β - 10.6 sin 2β |
| 33 | 44.4 | 16.8 | -13.3 | -8.9 | -1.11 - 19.2 cos 2β - 5.7 sin 2β | | 2 | 94.8 | -4.8 - 82.8 cos 2β - 24.5 sin 2β |
| 45 | 47 | 11.9 | -16.8 | 0.94 | 1.55 - 18.3 cos 2β + 0.6 sin 2β | | 2 | 95.9 | 6.75 - 79.7 cos 2β + 2.61 sin 2β |

Table I

c) Improvements of the model : anisotropic stress calculation, effects of plate thickness

Introduction of anisotropy in the determination of the mechanical bias

The force-frequency effect in a circular disk according to the isotropic stress calculation is given by

$$\frac{\Delta F}{F_o} = - \frac{2P}{\pi dt} \left((s_{a_{11}} + s_{a_{33}}) + 2(s_{a_{11}} + s_{a_{33}}) \cos 2\beta - 2s_{a_{11}} \sin 2\beta \right) \quad (24)$$

where

P is the applied force along a diameter

d is the diameter and t the thickness of the disk

$s_{a_{11}}$, $s_{a_{33}}$, $s_{a_{13}}$ are the in-plane coefficients expressed in the axes (a_1, a_3) parallel to the SAW

β is the azimuthal angle between the SAW and the force (Fig. 7).

The simple geometry of the circular disk allows an exact evaluation of the quasi-static mechanical bias at the center, taking into account quartz anisotropy.

According to Janiaud's anisotropic calculation [16], the stress distribution is still a simple radial distribution and its expression at the center of the plate is :

$$\bar{T}_{11}^o(\beta + \psi) = \frac{\rho\delta}{\pi dt} \left(\frac{4A}{\delta + \varepsilon + \zeta} - \frac{A+B}{\delta - \zeta + \gamma} \right) \quad (25)$$

$$\bar{T}_{33}^o(\beta + \psi) = - \frac{\rho\delta}{\pi dt} \left(\frac{A+B}{\delta - \zeta + \gamma} \right) \quad (26)$$

$$\bar{T}_{13}^o = 0 \quad (27)$$

where β is the azimuthal angle between the SAW and the force (Fig. 7)

ψ is the propagation angle of the SAW

($\varepsilon, \zeta, \gamma, \delta$ are the following combinations of compliance constants expressed in the axes (a_1^o, a_3^o))

$$\varepsilon = 4(S_{11} - S_{33}) \quad (28)$$

$$\zeta = S_{11} + S_{33} - 2S_{13} - S_{55} \quad (29)$$

$$\gamma = 4(S_{15} + S_{35}) \quad (30)$$

$$\delta = 2S_{13} + S_{55} + 3S_{33} + 3S_{11} \quad (31)$$

Coefficients A and B are determined numerically by the static equilibrium conditions for the plate. These coefficients depend on crystal anisotropy and are computed for each set of cut angles (Φ, θ) and propagation direction Ψ .

Final expression of the relative frequency shifts for a single diametral compression of magnitude P is

$$\begin{aligned} \frac{\Delta F}{F_0} = & \left(\frac{\bar{T}_{11}^o(\beta + \Psi) + \bar{T}_{33}^o(\beta + \Psi)}{2} \right) (s_{a_{11}} + s_{a_{33}}) \\ & + (s_{a_{11}} + s_{a_{33}}) \left(\frac{\bar{T}_{11}^o(\beta + \Psi) - \bar{T}_{33}^o(\beta + \Psi)}{2} \right) \cos 2\beta \\ & - s_{a_{13}} \left(\frac{\bar{T}_{11}^o(\beta + \Psi) - \bar{T}_{33}^o(\beta + \Psi)}{2} \right) \sin 2\beta \end{aligned} \quad (32)$$

In that case, the "mean value" corresponding to a 4-point symmetrical compression of magnitude $P/2$ is no longer independent of the angles β and Ψ and is given by

$$\frac{\Delta F}{F_0} = \left(\frac{\bar{T}_{11}^o(\beta + \Psi) + \bar{T}_{33}^o(\beta + \Psi)}{2} \right) (s_{a_{11}} + s_{a_{33}}) \quad (33)$$

Comparison between isotropic and anisotropic stress calculation is shown on Fig. 13 where solid lines represent theoretical values of the anisotropic stress calculation (broken lines = isotropic calculation).

The difference between the two models depends on the crystal cut. In the case of the ST-cut (Fig. 13a) the anisotropic model predicts a well-marked oscillation in the case of a 4-point compression. The average value of the oscillation corresponds to a constant value given by the isotropic stress calculation.

The difference between the two models is also significative in the case of Fig. 13b ($\Phi = 0, \theta = 41.8, \Psi = 48.2$). In the case of the cuts ($\Phi = 0, \theta \approx -10^\circ, \Psi \approx 30^\circ$) the two models predict almost the same result, and do not explain the discrepancy in amplitude and phase between theory and experiment on Fig. 13c. Fig. 13d shows the investigation on a thicker plate (2 mm thick) with a better agreement between theory and experiment ; this could be explained by a significant reduction of parasitic bending forces with respect to the previous experiments (1 mm thick).

Table 2 summarizes the experimental results obtained.

| | $\theta = -10^\circ$ $\psi = 30^\circ$ | $\theta = 41.8^\circ$ $\psi = 48.2^\circ$ | ST, $\theta = 42.75^\circ$ X $\psi = 0^\circ$ | |
|--|---|---|---|------------|
| coupling factor $\Delta V/V$ | 4.9×10^{-4} | 4.5×10^{-4} | 5.8×10^{-4} | THEORY |
| beam steering angle | -5.7° | $\simeq 6^\circ$ | 0 | |
| 2-nd order temperature coefficient | $-30 \times 10^{-9} \text{ K}^{-2}$ | $-30 \times 10^{-9} \text{ K}^{-2}$ | $-34 \times 10^{-9} \text{ K}^{-2}$ | EXPERIMENT |
| sensitivity to planar isotropic stresses | $< 3 \times 10^{-12} \text{ m}^2 \cdot \text{N}^{-1}$ | $< 5 \times 10^{-12} \text{ m}^2 \cdot \text{N}^{-1}$ | $\simeq 12 \times 10^{-12} \text{ m}^2 \cdot \text{N}^{-1}$ | |

Table 2

Through this model, the last step, at the present time, of analytical calculation has been reached for diametral in-plane compression.

As announced in the second interim progress report [26] numerical analysis by finite element method were implemented.

d) Comparison with results obtained by finite element analysis

Up to confirm previous predictions, particularly when anisotropy is held into account, finite element model have been coupled with the SAW calculation program in two manners :

- with stress sensitivity coefficients
- with complete integral expression of the perturbation method.

Since the compression is supposed to be homogeneous along the thickness, the present model is in two dimensions (Fig. 15). As in experiments (Fig. 7), the bottom of the plate is fixed and forces are applied at its top. The elastic constants used for calculation are C_{11} , C_{13} , C_{15} , C_{33} , C_{35} , C_{55} and the direction of propagation ψ is incremented with a 5° step up to simulate the azimuthal angle β between ψ and force direction as in experiments.

$$\frac{\Delta V}{V_0} = \frac{\sum_{r,s} A_r^* A_s \frac{\partial u_i^{(r)*}}{\partial u_j^{(s)}} n_k^{(r)*} n_m^{(s)} \sum_e \left(\overline{H_{ikjm}}(e) \times S(e) / (n_2^{(r)*} - n_2^{(s)}) \right)}{2 \rho_0 V_0^2 \sum_{r,s} A_r^* A_s \frac{\partial u_i^{(r)*}}{\partial u_j^{(s)}} \sum_e \left(S(e) / (n_2^{(r)*} - n_2^{(s)}) \right)} \quad (34)$$

where e represents the number of the current element, $S(e)$ its surface and $H_{ikjm}(e)$ the mechanical prestrained tensor for the element. In the case of isosurface for elements, the term $S(e)$ is equal to unity.

Computations were made for (ST,X) cut (Fig. 16).

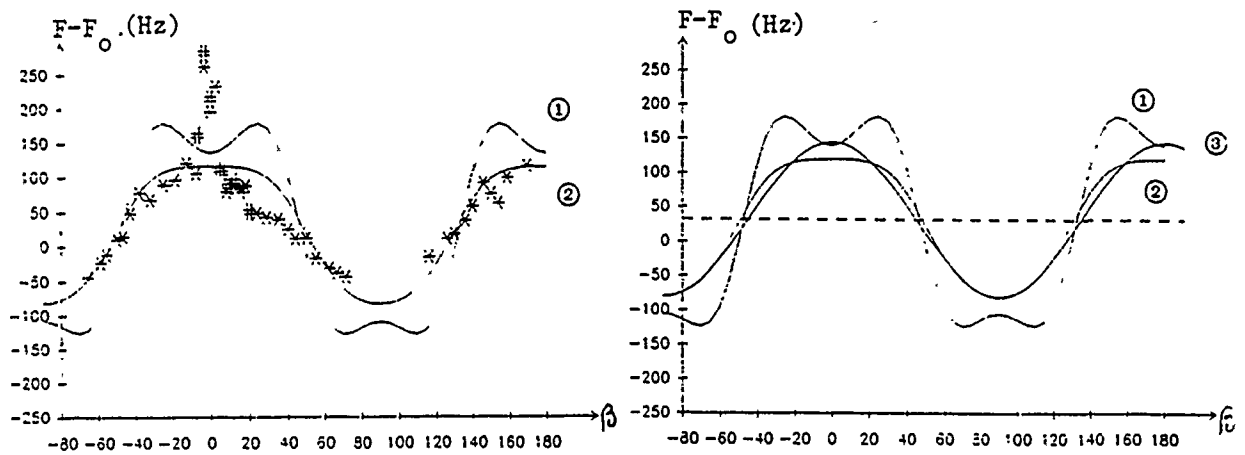


Fig. 16
Finite elements analysis results for (ST,X) cut
a : comparison with experimental measurements
b : comparison with analytical isotropic model
① complete coupling between finite element and perturbation methods
② calculation using stress sensitivity coefficients
③ classical isotropic model

As in anisotropic analytic model, a strong oscillation appears for (ST,X) cut with the complete reckoning, that seems to valid previous computations. This effect is also present when using stress sensitivity coefficients, but very smoother than the previous one. It can be also noted that the magnitude in the first case is much important than experimental results. This might be explained by strict restrictions on displacement used to resolve the static mechanical problem, and also the fact that interpolation polynomials are of degree 1, that yields to significative errors for the model. Presently, calculation with polynomials of 2nd degree is implemented.

As a conclusion of this chapter, one can establish that analytical and numerical results are in good agreement, and also with most of experimental ones.

Classical isotropic model can be used to choose a cut for its mechanical properties. More complete reckoning permits to improve simple models for a given structure. The isotropic model has been numerically implemented to test the compatibility between finite elements datas and the SAW program. It results that such a manner to calculate relative frequency shifts seems better than the stress coefficients calculation method. This phenomena is perhaps due to cumulative errors along the systematic tensorial calculation.

4 - EXPERIMENTAL STUDY OF DYNAMICAL TEMPERATURE EFFECTS

In this part, the frequency instability due to dynamical temperature perturbations is studied in reference to previous works about this subject [23-24].

It has been shown that mounting design has an important influence on the thermal sensitivity. A strong analytical effort has been made for demonstrate the existence of cuts insensitive to dynamic thermal effects, and yields to the conclusion that radial thermal conductivity may induce more frequency shifts than thickness conductivity in identical heating conditions [24]. Particularly, a two-dimension isotropic model was established, giving the time dependent distribution in a circular plate. Nevertheless, the solution obtained was really cumbersome and not of practical interest in SAW device modellings.

So, an experimental investigation has been presently choosen for the previous cuts mechanically tested (§ 3), with the idea that dynamic thermal perturbation within the plate has a similar behaviour as for stress sensitivity previously studied, but with a better accuracy.

The SAW frequency-temperature variation law, given by [23]

$$\frac{\Delta f}{f_0} = a_0 (T - T_0) + b_0 (T - T_0)^2 + \tilde{\alpha} \frac{dT}{dt} \quad (35)$$

where a_0 , b_0 are respectively the first and second order static temperature coefficients and α the dynamic temperature coefficient, reduces to

$$\left(\frac{\Delta f}{f_0} \right)_{dyn} = \tilde{\alpha} \frac{dT}{dt} \quad (36)$$

when the device is just around temperature T_0 .

This model shows that the relative frequency shift due to dynamic temperature effect is proportional to the thermal excitation speed.

a) Experimental method

In fact, when a SAW resonator is submitted to dynamic temperature biases, the whole enclosure is excited and the thermal wave is assumed to propagate mainly via the mounting of the quartz plate. To obtain such experimental effects, a supply

has been built composed of a copper plate (chosen for its good thermal conductivity) with a ceramic case NPN transistor fixed on its bottom (Fig. 17).

Two mountings, supporting the quartz plate, are attached on the top of the copper plate permitting thermal excitation of the SAW propagating substrate. The whole system is placed in a brass case electrically referred to zero potential (Fig. 18) with no thermal conductivity between the enclosure and the SAW device.

Two resistive sensors, one fixed under the quartz plate and the other one on one of the mountings, give the temperature variations. This device and the loop amplifier are at the initial temperature of -30°C up to permit thermal cycles approximatively around ambient temperature (18 to 25°C). The experiment is controlled by a program that commands the electric excitation of the transistor and stores temperature and frequency data during cycles. Each experiment is made with a significative number of temperature cycles, that yields to obtain repetitive measurements around a steady state.

b) Results

Classical (ST, X) cut and a single-rotated, close to TG, cut ($\phi = 0^{\circ}$, $\theta = -7^{\circ}$, $\Psi = 31^{\circ}$) have been tested, and comparison is made between results. First, we verify that experimental conditions of dynamic temperature tests were present by cycling both cuts at different magnitude of thermal excitation, for a fixed cycling time. Results are shown in Table III.

Comparison between the two cuts behaviour is possible, and we showed (Fig. 19) that ($\phi = 0^{\circ}$, $\theta = -7^{\circ}$, $\Psi = 31^{\circ}$) cut is about ten times less sensitive than (ST,X) cut, that seems to confirm previous assumptions on stress sensitivity.

It has been demonstrated that temperature behaviour is an accurate method to determine the best insensitive cut for SAW device applications. Nevertheless, this method needs a heavy setup to obtain the sensitivity and it could be interesting to develop numerical modelings to predict the sensitivity, taking into account the right design.

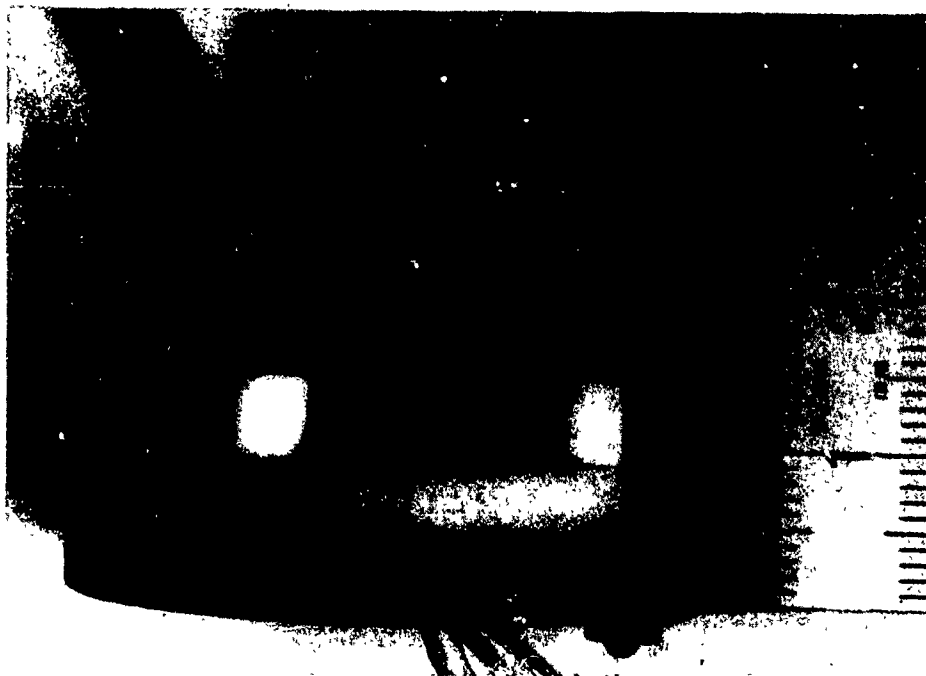


Fig. 17 : Heating device for dynamic thermal sensitivity measurements



Fig. 18 : The SAW delay line is mounted in a brass enclosure with a good thermal insulation

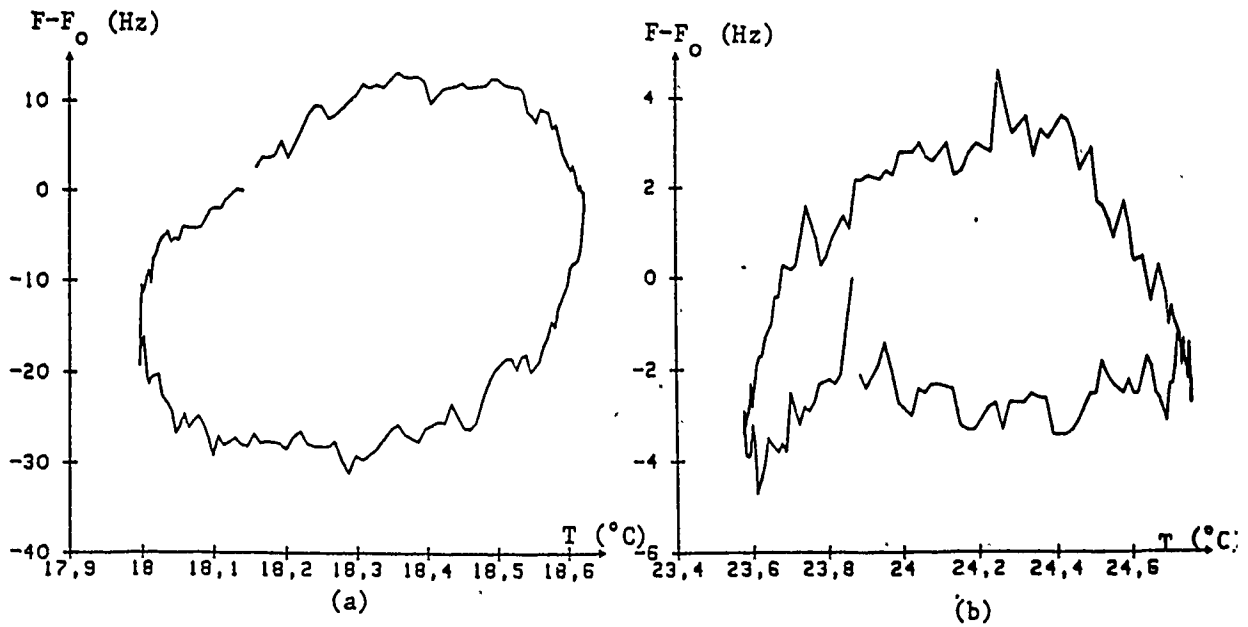


Fig. 19 : Comparison between (ST,X) cut (a) and $(\phi = 0^\circ, \theta = -7^\circ, \Psi = 31^\circ)$ cut (b)
 cycle duration : 180 s
 number of measurements : 171
 Fixation points are the in-plane stress insensitive ones

| (ST, X) cut | | $(\phi = 0^\circ; \theta = -7^\circ; \Psi = 31^\circ)$ cut | |
|--|--|--|--|
| cycling speed in $^\circ\text{K}/\text{mn}$ | $(F-F_0)_{\text{max}} - (F-F_0)_{\text{min}}$ in Hz | cycling speed in $^\circ\text{K}/\text{mn}$ | $(F-F_0)_{\text{max}} - (F-F_0)_{\text{min}}$ in Hz |
| 0.203 | 19.5 | 0.388 | 4.3 |
| 0.399 | 39.3 | 0.433 | 4.6 |
| 0.612 | 58.5 | 0.788 | 9.3 |

Table 3

After the results of this table, dynamic thermal coefficient \tilde{a} of the two cuts can be evaluated.

For ST-cut \tilde{a} is equal to $1.10^{-6} \text{ s}/^\circ\text{K}$ and the $(\phi = 0^\circ, \theta = -7^\circ, \Psi = 31^\circ)$ cut has a dynamic thermal coefficient a equal to $.11.10^{-6}$, then ten times lower than for the usual quartz cut.

This confirms the stress sensitivity calculated in the third chapter.

5. CALCULATIONS ON FLEXURAL SENSITIVITY OF SAW QUARTZ CUTS COMPENSATED FOR PLANAR ISOTROPIC STRESSES

In this section, the behaviour of a SAW device built on a quartz plate submitted to bending forces will be examined. The simple case of a rectangular plate, either clamped at one end and loaded at the other (cantilever beam) or clamped on two edges and submitted to a normal acceleration, and the case of the same plate subjected to equal and opposite bending moments at its ends are presented. In the two first approaches, stress distributions will be calculated in the classical model of the isotropic thin plate [21], and their influence on SAW propagation will be calculated according to the model of stress sensitivity coefficients.

The last one consists in a complete anisotropic modelling for stresses, strains and displacement gradients, and the numerical processing established to couple finite element method and SAW program will be used to calculate the frequency shift.

In all these cases, the fixation points are supposed to be "not too close" to the SAW propagating beam, so boundary effects can be neglected (St Venant principle).

a) classical isotropic stress calculations

Let us consider the case of the isotropic cantilever beam. The width of the plate is supposed infinite and the loading force homogeneous. So, in agreement with classical thin plate theory [21], the problem reduces to the resolution of a two-dimension differential equation which expression is

$$\frac{\partial^4 \phi}{\partial a_1^4} + 2 \frac{\partial^4 \phi}{\partial a_1^2 \partial a_2^2} + \frac{\partial^4 \phi}{\partial a_2^4} = 0 \quad (37)$$

with ϕ the stress function related to stresses by the relations

$$\overline{T_{11}} = \frac{\partial^2 \phi}{\partial a_2^2} ; \quad \overline{T_{22}} = \frac{\partial^2 \phi}{\partial a_1^2} ; \quad \overline{T_{12}} = - \frac{\partial^2 \phi}{\partial a_1 \partial a_2} \quad (38)$$

where the absence of body forces is assumed (Fig. 20).

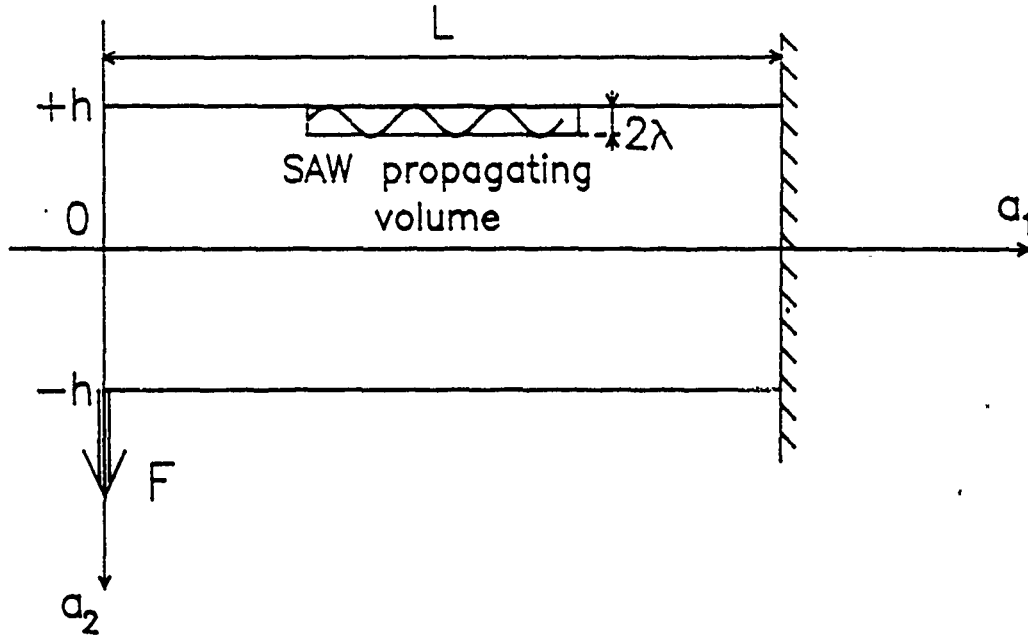


Fig. 20 : Stresses in a cantilever beam clamped at one end

In such a case, solution of eq. (37) in the form of polynomials is of interest. Having regard to boundary conditions which are :

- no stresses on longitudinal sides $\pm h$
- the sum of the shearing forces distributed over the loaded end must be equal to F
- T_{11} must be equal to zero at the loaded end (no compressive stress in the a_1 direction at the loaded end) and taking the stress function in the form of a polynomial of fourth degree yield to the following solution

$$\overline{T_{11}^o} = \frac{3F}{2h^3} a_1 a_2 \quad ; \quad \overline{T_{12}^o} = - \frac{3F}{2h^3} (a_2^2 - h^2) \quad (39)$$

By integrating these expressions over the SAW propagating volume, and then dividing the results by the value of this volume, the mean values of stresses that perturbate SAW propagation are obtained. Using a perturbation method with the hypothesis of no rigid rotation of the plate (after application of static bias), the frequency shift is given by

$$\left\langle \frac{\Delta\omega}{\omega_o} \right\rangle = s_{a_{11}} \left\langle \overline{T_{11}^o} \right\rangle + s_{a_{12}} \left\langle \overline{T_{12}^o} \right\rangle \quad (40)$$

where $\langle \rangle$ stands for the mean value over the volume where the SAW propagates.

In eq. (40) the loading force is applied along the propagation direction.

The model of cantilever beam has been used for SAW accelerometer applications, but the case of a rectangular plate clamped on two edges and bent by its own weight (which corresponds to the case of quasi-static normal accelerations) is probably more realistic for the modelization of SAW oscillators.

The calculation process is the same as the previous one, except that a polynomial of the fifth degree is chosen for the stress function and the boundary conditions are :

- the plate is sunk at its two ends
- there is no normal stresses acting on the longitudinal sides
- there is no flexural moments applied at $\pm \ell$ (Fig. 21).

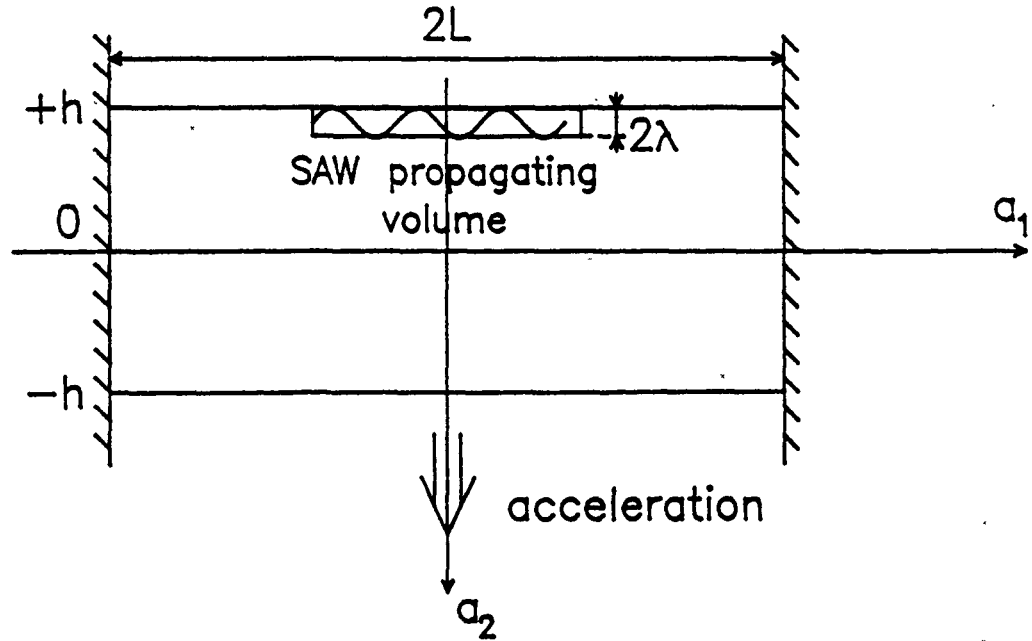


Fig. 21

Solutions respecting boundary conditions given by the classical theory of elasticity [17] yield the following expressions of stresses

$$\overline{T_{11}^o} = -\frac{3\rho g}{2h^2} (a_1^2 a_2 - \frac{2}{3} a_2^3) + \frac{3}{2} \rho g \left(\frac{\ell^2}{h^2} - \frac{2}{5} \right) a_2 \quad (41)$$

$$\overline{T_{22}^o} = -\left(\frac{\rho g}{2h^2} \right) a_2^3 + \frac{\rho g}{2} a_2 \quad (42)$$

$$\overline{T_{12}^o} = \frac{3\rho g}{2h^2} a_1 a_2^2 - \frac{3\rho g}{2} a_1 \quad (43)$$

The relative velocity shifts of the SAW will be expressed (using a similar notation as in eq. (40) by

$$\left\langle \frac{\Delta\omega}{\omega_0} \right\rangle = s_{a_{11}} \left\langle \overline{T_{11}^o} \right\rangle + s_{a_{22}} \left\langle \overline{T_{22}^o} \right\rangle \quad (44)$$

In eq. (44) the contribution of the shear component $\langle \overline{T_{12}^o} \rangle$ vanishes by symmetry. Eqs. (40) and (44) therefore exhibit a similar form combining an in-plane compressive stress $\langle \overline{T_{11}^o} \rangle$ and a second term either due to a shear component (plate clamped at one end) or to a normal compressive stress (plate submitted to a normal acceleration).

An important fact to point out is that if the main contribution is due to the term $s_{a_{11}} \langle \overline{T_{11}^o} \rangle$, flexural sensitivity will be equivalent to in-plane stress sensitivity. Under this assumption, a device built with a cut compensated for planar isotropic stresses will also exhibit a low sensitivity to a symmetrical distribution of flexural stresses.

b) Anisotropic stress model

Timoshenko and Goodier [21] established that a 3-dimensional elasticity problem can be modelised with equilibrium equations and boundary conditions for stress components either constant or linearly dependent of coordinates, so the compatibility equations are identically respected, and the stresses are correct solutions of the problem. If the stress distribution is assumed to be as follows

$$\overline{T_{11}^o} = \frac{M}{I} a_2 ; \quad \overline{T_{22}^o} = \overline{T_{33}^o} = \overline{T_{13}^o} = \overline{T_{12}^o} = \overline{T_{23}^o} = 0 \quad (45)$$

with I the moment of inertia, M the bending moment and a_2 the thickness coordinate (Fig. 22), we showed that anisotropy could be introduced for calculating strains and displacements without complication for the model.

The reckoning procedure is quite the same as exposed in [21] and yields to the following results :

$$\overline{S}_{ij}^o = s_{ij11} \overline{T}_{11}^o$$

$$\overline{u}_1^o = \frac{M}{I} a_2 (s_{11} a_1 + s_{51} a_2)$$

(46)

$$\overline{u}_2^o = \frac{M}{I} \left[(s_{61} + \frac{s_{11}}{2}) a_1^2 - s_{51} a_1 a_3 + \frac{s_{21}}{2} a_2^2 - \frac{s_{31}}{2} a_3^2 \right]$$

$$\overline{u}_3^o = \frac{M}{I} \left[s_{51} a_2 a_1 + s_{31} a_2 a_3 + s_{41} a_2^2 \right]$$

where conditions of fixed point in the center of the plate and no rigid rotations around it have been imposed up to assure the unicity of the solution.

Values for stresses, strains and displacement gradients have been calculated in the propagation area for a certain number of small parallelepipedic elements (Fig. 23), and then introduced in the perturbation method. Fig. 26 shows the results for (ST,X), experimental STC and TG (-10, 30) cuts, which seems to confirm the possibility of very low sensitivity to flexural effects and especially for TG cut.

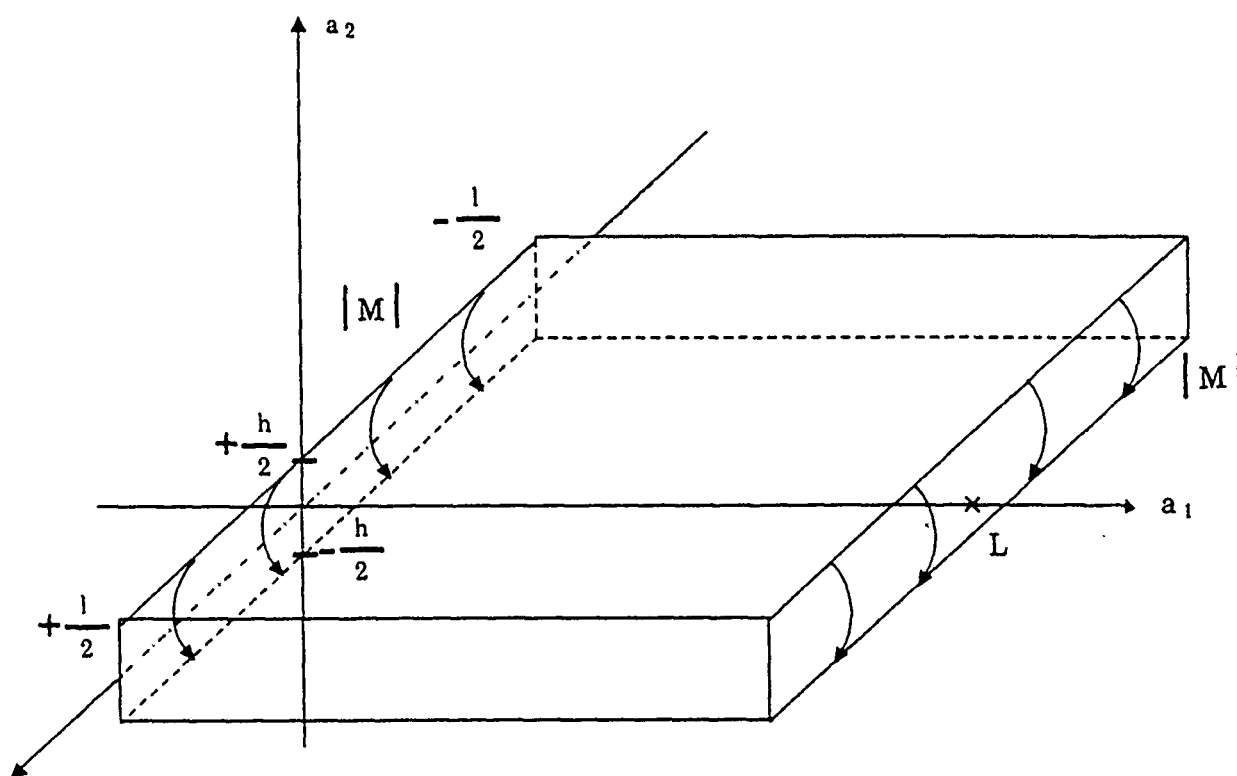


Fig. 22
Thin quartz plate submitted to equal and opposite bending moment M
dimensions : $h = 1 \text{ mm}$; $\ell = L = 22 \text{ mm}$

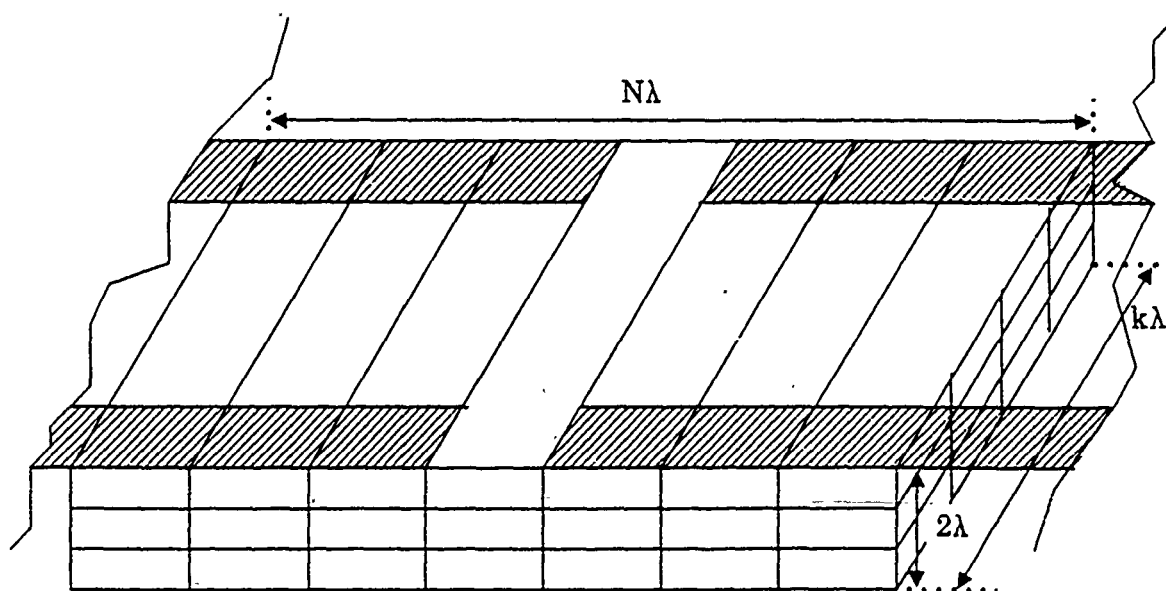


Fig. 23
SAW propagating volume subdivided in small parallelepipedic elements
(with λ the wavelength)

c) Numerical results of the cuts (P30), (P45) and (ST,X)

The flexural effect was calculated for a device built on a rectangular plate with some realistic values

plate length : 17 mm \rightarrow 22 mm

thickness : 2 mm

wavelength : 34.4 μ m

wavelength/thickness ratio : 1.7×10^{-2}

Results are presented on Fig. 24 for the plate clamped at one edge and on Fig. 25 for the plate clamped on two edges and submitted to a normal acceleration. Results are expressed in terms of relative velocity shifts (normalized to the mean value of compressive strains $\langle \overline{S}_{11} \rangle = s_{1111} \langle \overline{T}_{11} \rangle$) as a function of the azimuthal angle β between the SAW propagation direction and the edges of the rectangular plate (Figs. 24a and 25a).

For the P30 and P45 cuts, the main contribution to the flexural effect is due to the compressive stress $\langle \overline{T}_{11} \rangle$. The sinusoidal shape of the curves on Figs. 24 and 25 may be interpreted simply as the tensorial transformation of stresses when turning the azimuthal angle β ; this behavior is very similar to the case of simple diametral compression calculated in sec. 3, Eq. (22).

Results obtained with the anisotropic model appear on Fig. 26. They show a strong similarity about the shape with the anisotropic radial in-planes sensitivity curves (section 3) and a general identical behaviour with previous isotropic models (because of the particular stress distribution, that is \overline{T}_{11} the only non-zero stress term).

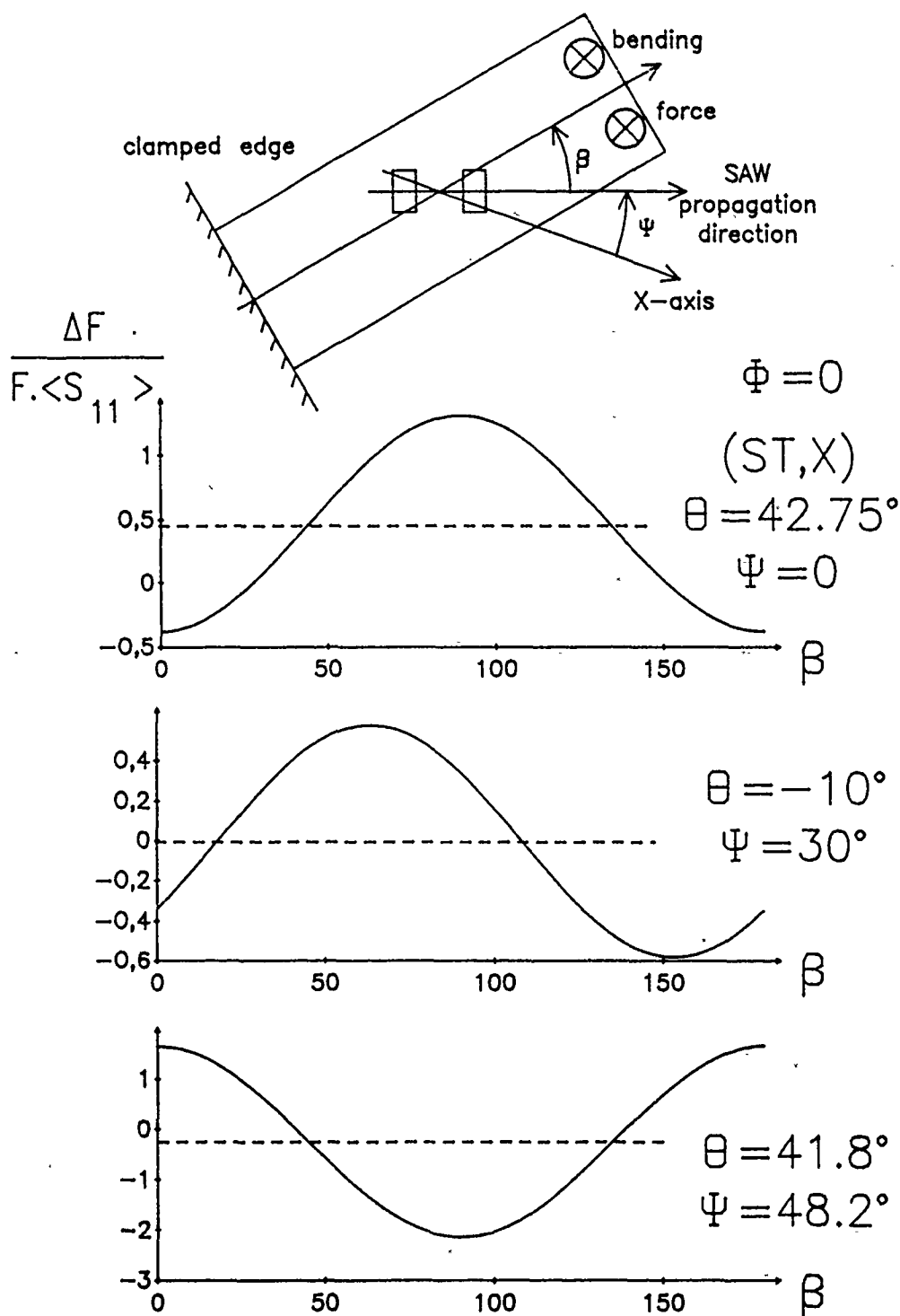


Fig. 24
 Flexural effects (isotropic stress model) for a SAW propagating
 on a bent cantilever beam
 dimensions : $L = 17 \text{ mm}$ thickness = 2 mm $\lambda = 34.4 \text{ } \mu\text{m}$
 a : definition of the azimuthal angle β
 b, c, d : comparison of planar isotropic stress compensated cuts
 with the classical (ST,X) cut

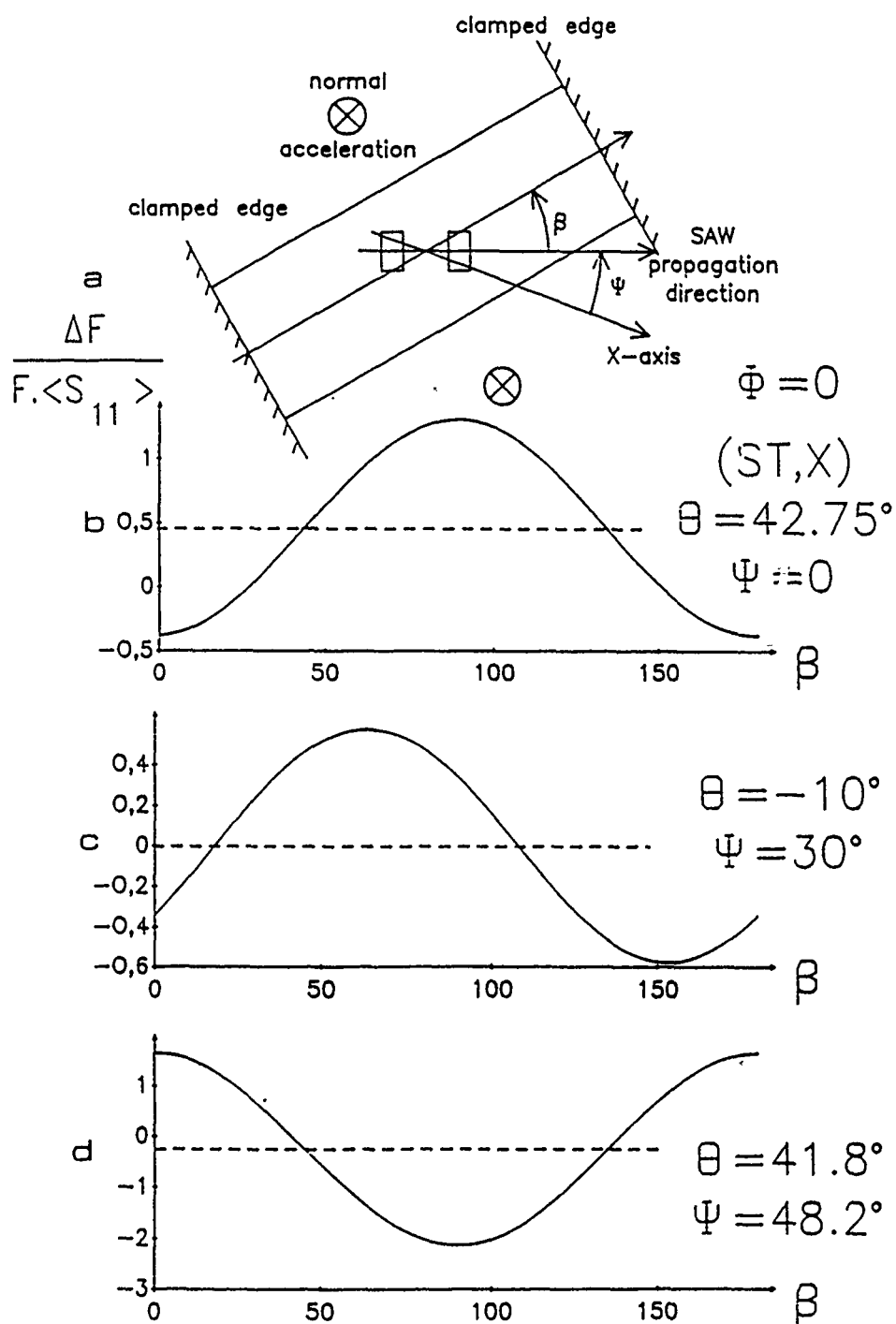


Fig. 25

Flexural effects for a SAW propagating on a plate clamped on both edges and submitted to a normal acceleration. Convention as in Fig. 16.

$2L = 22 \text{ mm}$ thickness $= 2 \text{ mm}$ $\lambda = 34,4 \mu\text{m}$

Similarity between Figs. 24 and 25 is due to the fact that the main contribution to the effect is due in both cases to compressive in plane stresses

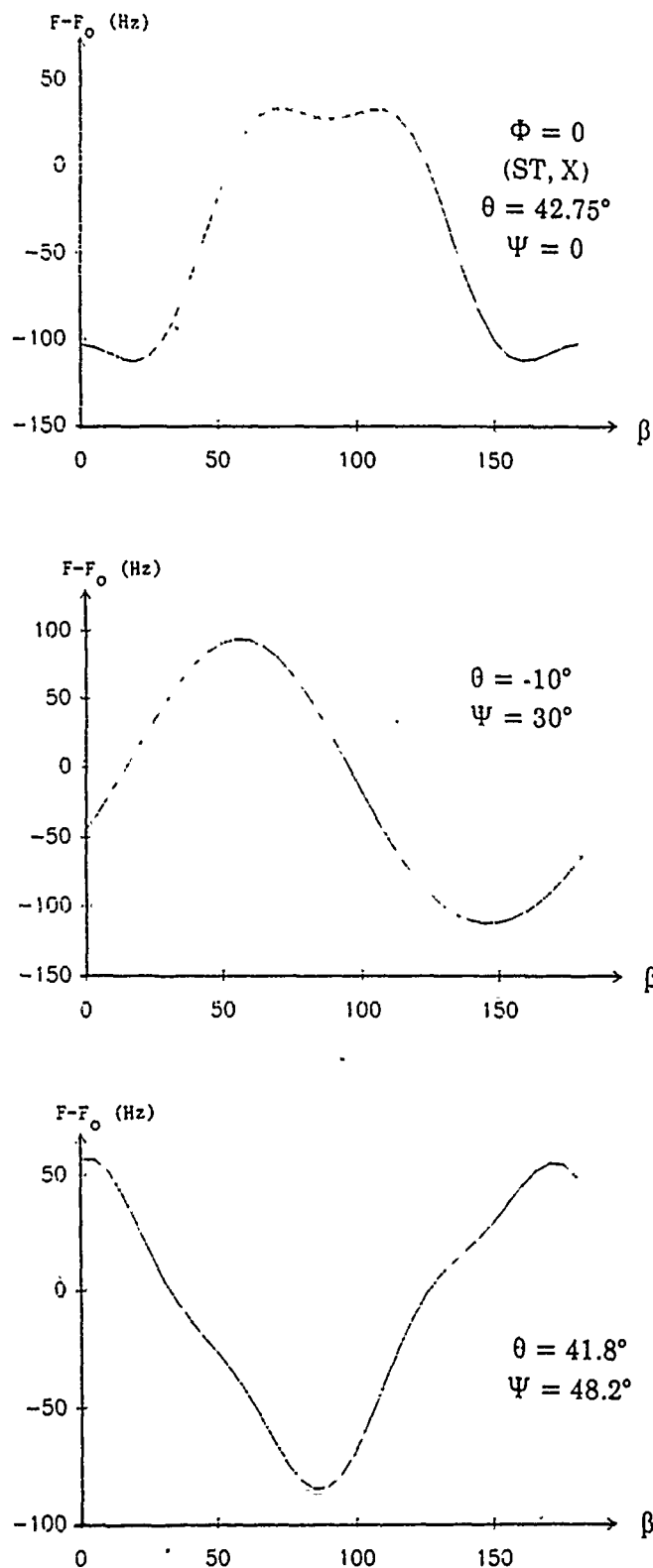


Fig. 26

Flexural effects for a SAW propagating on a quartz plate submitted to equal and opposite bending moments M . These results are very closed to previous bending effect models and to compressive in-plane anisotropic model because of the particular stress distribution

For a suitable choice of the angle β , the device will be insensitive to flexural effects. In the case of the P30 and P45 cuts, there is no offset value of the sinusoidal curve, and therefore the device will be insensitive to a symmetrical distribution of bending stresses : this will happen if the two principal compressive stresses \overline{T}_{11} and \overline{T}_{33} are equal and with same sign ; the contribution of other stresses such as \overline{T}_{12} , \overline{T}_{32} , \overline{T}_{22} being of much lower magnitude.

CONCLUSION

Experimental measurements have been extended in the vicinity of the P45 cut, close to B.K. Sinha's STC-cut [14]. The following cuts ($\phi = 0^\circ$, $\theta = 39^\circ$, $\Psi = 46^\circ$), ($\phi = 0^\circ$, $\theta = 33^\circ$, $\Psi = 44.4^\circ$), ($\phi = 0^\circ$, $\theta = 45^\circ$, $\Psi = 47^\circ$) have been experimentally found to be temperature-compensated (by small correction on the propagation direction Ψ relatively to the theoretical values given by computation) and then mechanically tested in radial in-plane compression experiment. During these manipulations, it has been shown as previously that reducing stress sensitivity by increasing thickness of the plate induces higher experimental dispersion of the results.

Finite element method has been employed in the calculation process of frequency shift. It was of major importance to valid the previous analytical anisotropic model. Results that have been obtained are rather in a good agreement with experiments for a two dimensions model. More, the tests implemented in order to establish the validity of the coupling between finite elements and SAW program showed that systematic calculations may introduce significative errors in the stress sensitivity coefficients calculation.

A dynamic thermal experiment was implemented. It has been shown that, depending on SAW orientations, it exists particular cuts which are less sensitive than others, or particularly than standard (ST,X) cut. That may yield to the realisation of SAW devices, insensitive to in-plane compression, flexion effects, statically and dynamically temperature-compensated, with a satisfying safety margin on cut angles especially in the vicinity of the P30-cut.

A new flexural anisotropic model was established with a good agreement between its results and the isotropic previous one, given in the 2nd interim progress. More, since St Venant's principle is assumed so that only compressive effects are of

importance in the plate center, the accordance between all the mechanical models is clearly demonstrated.

Of course, we must purchase our investigations, particularly for dynamic thermal effect experiments and computations, that are now possible by the use of finite element program MODULEF (by courtesy of Mr. Crolet, Director of the L.C.S.; Besançon, France). We will investigate the time dependent thermal distribution in a 3 dimensions anisotropic plate and the stresses due to a dynamic temperature excitation.

We will also attempt to work on higher precision quartz devices, up to confirm the analytical predictions, and cuts in the vicinity of P45 cut will be thermally experimented.

Also classical quartz lines used for the previous experiments should be replaced by real resonators, that would introduce some modifications in the theoretical approach of phenomena.

The different points can merge into a general method to define the whole structure of a low sensitive SAW device for military or space applications.

APPENDIX 1

CUT ANGLES AND PROPAGATION DIRECTION FOR SAWs ON QUARTZ DEFINITION AND SYMMETRY PROPERTIES

1 - Correspondance between IEEE and Euler notation

Fig. 27 defines angles [16] and Euler angles according to Rosenberg [25].

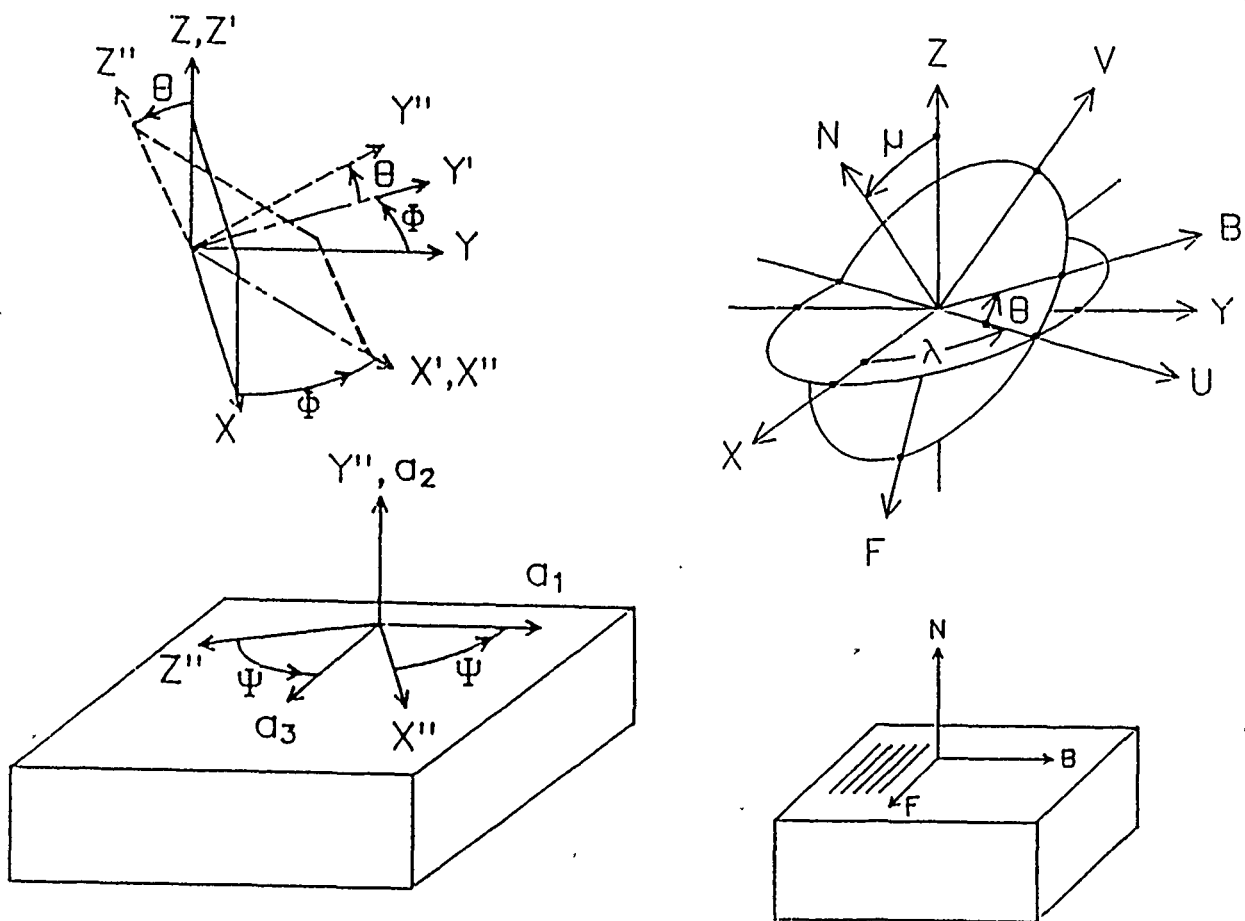


Fig. 27 : Correspondance between IEEE and Euler angles

Correspondance between the two angles is obtained by identifying the unit vectors (a_1, a_2, a_3) defined by IEEE angles and (B, N, F) vectors using Rosenberg's notation for Euler angles.

The only difference appears in the definition of the second angle θ_{IEEE} or μ_{Euler} , the first referring to the plate surface and the second to the plate normal. Thus, the correspondance is simply :

$$\lambda_{Euler} = \Phi_{IEEE} \quad (A.1)$$

$$\mu_{Euler} = \theta_{IEEE} - 90^\circ \quad (A.2)$$

$$\theta_{Euler} = \Psi_{IEEE} \quad (A.3)$$

2 - Symmetry properties (IEEE notation)

Surface waves on quartz obey the three following symmetries.

a) Redundancy in the definition of the cut angles

From the definition of the cut angles, the following symmetry property appears :

$$(\phi, \theta, \psi) = (\phi + 180^\circ, 180^\circ - \theta, \psi + 180^\circ) \quad (A.4)$$

b) Symmetries of quartz

- 3-fold symmetry around the Z-axis

$$(\phi, \theta, \psi) = (\phi + 120^\circ, \theta, \psi) \quad (A.5)$$

- 2-fold symmetry around X-axis

$$(\phi, \theta, \psi) = (-\phi, \theta + 180^\circ, \psi) \quad (A.6)$$

Combination of (29) and (27) yields an equivalent form

$$(\phi, \theta, \psi) = (180^\circ - \phi, -\theta, 180^\circ + \psi) \quad (A.7)$$

c) Symmetries of surface waves

Two surface waves on the same plate have the same properties in case of :

- propagation on the same surface, with opposite directions

$$(\phi, \theta, \psi) = (\phi, \theta, \psi + 180^\circ) \quad (A.8)$$

- propagation in the same direction, but on the other side of the plate

$$(\phi, \theta, \psi) = (\phi, \theta + 180^\circ, -\psi) \quad (A.9)$$

Eqs. (A.8) and (A.9) come from the symmetry of the determinants that define the surface wave parameters.

Combination of (A.6) and (A.9) yields the equivalent form

$$(\phi, \theta, \psi) = (-\phi, \theta, -\Psi) \quad (\text{A.10})$$

d) Consequences on the angular range required for a complete stress and temperature coefficients mapping

Starting from the most general angular range : $0 \rightarrow 360^\circ$ for the three angles, the three symmetries a) b) and c) yield

- eq. (A.4) reduces the angular range on θ to $-90^\circ \rightarrow +90^\circ$
- eq. (A.5) reduces the angular range on ϕ to $-60^\circ \rightarrow +60^\circ$
- eq. (A.7) reduces the angular range on θ from $-90 \rightarrow +90^\circ$ to $0 \rightarrow +90^\circ$
- eqs. (A.8) and (A.9) reduce the angular range on ψ to $0 \rightarrow 90^\circ$.

The combination of (A.5), (A.7), (A.8) yields :

$$(\phi, \theta, \psi) = (60^\circ - \phi, -\theta, \Psi) \quad (\text{A.11})$$

$$(\phi, \theta, \psi) = (-60^\circ - \phi, -\theta, \Psi) \quad (\text{A.12})$$

Eqs. (A.11) and (A.12) show that the points $(\phi = +30^\circ, \theta = 0)$ and $(\phi = -30^\circ, \theta = 0)$ are centers of symmetry for the contour-lines on Figs. 4 and 5.

3 - Correspondance between IRE-1949 and IEEE-1978 standards on piezoelectricity

In 1978, the IEEE standard on piezoelectricity [27] changed the orientation of the canonical axes of quartz, so that the definition for quartz should be coherent with other crystals. The consequence of this change is a rotation of the canonical axes by 180° around the Z-axis i.e. : $X \rightarrow -X, Y \rightarrow -Y$.

Most of authors still refer to the "old" 1949-standard which is taken as the reference in this work. Correspondance between the two standards is as follows : a cut defined by the angles (ϕ, θ, ψ) in the 1949-standard will be the same if defined by the angles $(\phi + 180^\circ, \theta, \psi)$ in the 1978-standard. Using symmetry equation (A.7) the correspondance between the two standards is finally :

$$1949\text{-cut}(\phi; \theta, \psi) = 1978\text{-cut}(-\phi, -\theta, \psi) \quad (\text{A.13})$$

For example : the ST-cut will be defined by $(\phi = 0, \theta = 42.75^\circ, \Psi = 0)$ in 1949-standard and by $(\phi = 0, \theta = -42.75^\circ, \Psi = 0)$ in the "new" 1978-standard.

REFERENCES

- [1] H.F. Tiersten and B.K. Sinha, "Temperature derivatives of the fundamental elastic constants of quartz", Proc. 32nd Ann. Freq. Cont. Symp., 1978, pp. 150-154.
- [2] D. Hauden, M. Michel and J.J. Gagnepain, "Higher order temperature coefficients of quartz SAW oscillators", Proc. 32nd Ann. Freq. Cont. Symp., 1978, pp. 77-86.
- [3] P. Levesque, M. Valdois, D. Hauden, J.J. Gagnepain, P. Hartemann, J. Uebersfeld, "Theoretical and experimental analysis of SAW quartz oscillator acceleration sensitivity", 1979 Ultrasonics Symp. Proc. IEEE, cat. 79CH1482-9SU.
- [4] J.F. Dias, H.E. Karrer, "Stress effects in acoustic surface wave circuits and applications to pressure and force transducers", IEEE Int. Conf. Solid-state Circuits, 1974.
- [5] H.F. Tiersten, D.S. Stevens, P.K. Das, "Acoustic surface wave accelerometer and rotation rate sensor", Proc. 1980 Ultrasonics Symp., IEEE cat. n° 80 CH 1602-2, pp. 692-695.
- [6] D. Hauden, S. Rousseau, J.J. Gagnepain, "Sensitivities of SAW oscillators to temperature, forces and pressure : application to sensors", Proc. 34th Ann. Freq. Cont. Symp., 1980.
- [7] T.M. Reeder, D.E. Cullen, M. Gilden, "SAW oscillator pressure sensors", Proc. 1975 Ultrasonics Symp., IEEE cat. n° 75 CHO 994, pp. 264-268.
- [8] P. Hartemann, P.L. Meunier, "Tensioned or flexured SAW accelerometers", 1983 Ultrasonics Symp. Proc. IEEE, cat. 83CH1947-1.
- [9] E. Bigler, G. Théobald and D. Hauden, "SAW quartz cuts with low stress and temperature sensitivity", Electron. Lett., vol. 23, n° 10, pp. 514-516, (may 1987).

- [10] E. Bigler, G. Théobald, D. Hauden, "Stress sensitivity mapping for surface acoustic waves on quartz", *IEEE Trans. Ultr. Ferro. Freq. Contr.*, vol. UFFC-36, n° 1, pp. 57-62 (jan. 1989).
- [11] E.P. Eernisse, "Calculations on the stress-compensated (SC-cut) quartz resonator", *Proc. 30th Ann. Freq. Cont. Symp.*, 1976, pp. 8-11.
- [12] H.F. Tiersten and J.C. Baumhauer, "Nonlinear electroelastic equations for small fields superposed on a bias", *J. Acoust. Soc. Am.*, 54, p. 1017, 1973.
- [13] H.F. Tiersten and B.K. Sinha, "A perturbation analysis of the attenuation and dispersion of surface waves", *J. Appl. Phys.*, 49, p. 87, 1978.
- [14] D. Hauden, M. Planat, J.J. Gagnepain, "Nonlinear properties of surface acoustic waves : applications on oscillators and sensors", *IEEE Trans. Sonics Ultrason.*, SU-18, n° 5, 1981.
- [15] J.J. Campbell and W.R. Jones, "A method for estimating optimal crystal cuts and propagation direction for excitation of piezoelectric surface waves", *IEEE Trans. Sonics Ultrason.*, SU-15, pp. 209-217, 1968.
- [16] IEEE Standard on Piezoelectricity 176-1949, *Proc. IRE*, vol. 37 (1949), pp. 1378-1395.
- [17] A.J. Slobodnik, E.D. Conway, R.T. Delmonico, "Microwave Acoustics Handbook, vol. 1A : Surface Wave Velocities", Air Force Cambridge Research Labs, 1973.
- [18] R. Bechmann, A.D. Ballato, T.J. Lukaszek, "Higher order temperature coefficients of the elastic stiffnesses and compliances of alpha-quartz", *Proc. IRE*, p. 1812, 1962.
- [19] R.N. Thurston, H.J. McSkimin, P. Andreacht, "Third-order elastic coefficients of quartz", *J. Appl. Phys.*, 37, pp. 267-275, 1966.
- [20] B.K. Sinha, "A stress and temperature compensated orientation and propagation direction for surface acoustic wave devices", *IEEE Trans. Ultrason. Ferro. Freq. Cont.*, vol. UFFC-34, n° 1, pp. 64-74 (jan. 1987).

- [21] S.P. Timoshenko and J.W Goodier, in "Theory of Elasticity", p. 122, 3rd edition (International Student Edition), McGrawHill, ed. (1970).
- [22] D. Janiaud, "Modélisation de l'influence d'une accélération sur la fréquence des résonateurs à quartz", Thèse, Université de Besançon, 1978, pp. 63-67.
- [23] D. Hauden, G. Théobald, "Dynamic thermal sensitivity of SAW quartz oscillators", 1980 Ultrasonics Symposium.
- [24] J.P. Valentin, G. Théobald, J.J. Gagnepain, "Frequency shift arising from in-plane temperature gradient distribution in quartz resonators", Proc. 38th Ann. Freq. Cont. Symp., Philadelphia, 1984.
- [25] R.L. Rosenberg, "Thermal shearing effects on the temperature stability of SAW devices", IEEE Trans. Son. Ultrasonics, SU-27, pp. 130-133, 1980.
- [26] E. Bigler, D. Hauden, S. Ballandras, "Stress and thermal stress compensation in quartz SAW devices", Interim Progress Report, 1 june 88 - 31 may 1989, Grant United States Air Force AFOSR-87-0241.
- [27] IEEE Standard on Piezoelectricity, 176-1978, IEEE Trans. Son. Ultrason., SU-31, n° 2, 1984.

**MISSION
OF
ROME LABORATORY**

Rome Laboratory plans and executes an interdisciplinary program in research, development, test, and technology transition in support of Air Force Command, Control, Communications and Intelligence (C³I) activities for all Air Force platforms. It also executes selected acquisition programs in several areas of expertise. Technical and engineering support within areas of competence is provided to ESD Program Offices (POs) and other ESD elements to perform effective acquisition of C³I systems. In addition, Rome Laboratory's technology supports other AFSC Product Divisions, the Air Force user community, and other DOD and non-DOD agencies. Rome Laboratory maintains technical competence and research programs in areas including, but not limited to, communications, command and control, battle management, intelligence information processing, computational sciences and software producibility, wide area surveillance/sensors, signal processing, solid state sciences, photonics, electromagnetic technology, superconductivity, and electronic reliability/maintainability and testability.